

POLITECNICO DI MILANO

CORSO DI LAUREA IN INGEGNERIA AERONAUTICA



Entrainment phenomena of paraffin-based fuels in
hybrid rocket engines combustion

Relatore:

Luciano Galfetti

F. Javier Loscertales Castaños

Matricola: 749479

Anno accademico 2011/2012

Abstract

The thesis is intended to investigate the entrainment phenomenon, simulating a flow of air parallel to a paraffin surface, in order to study the effect of different velocity profiles in the formation of droplets of paraffin in the above-mentioned flow. The effect is measured in terms of number of droplets and their sizes, being parameters that determine the regression rate in hybrid rockets which is one of the most important parameters in the performance of the rocket engines. The used tool is Gerris which is a free software program for the solution of the partial differential equations describing a fluid flow and allows the study of multiphase flows through a Volume of Fluid Method which is a numerical technique for tracking and locating interfaces, in particular fluid-fluid ones.

Contents

1	Introduction	8
1.1	Motivations	8
1.2	Objectives	9
1.3	Outline	9
2	Hybrid Rocket Propulsion	11
2.1	Introduction	11
2.2	A short summary about the history of hybrid rockets	12
2.3	Advantages and disadvantages of hybrid propulsion	14
2.3.1	Advantages compared with bipropellant liquid propulsion:	14
2.3.2	Advantages compared with solid propulsion:	14
2.3.3	Disadvantages of hybrid propulsion:	14
3	Properties of paraffin-based fuels	16
3.1	Liquefying hybrid fuels	16
3.2	Paraffin wax	18
4	Gerris Model	20
4.1	General characteristics of the Gerris code	21
4.1.1	The domain	22
4.1.2	The boundary conditions	22
4.1.3	The refinement	23

4.1.4	The time	25
4.1.5	The output of the code	26
4.1.6	Initial Conditions	27
4.1.7	Physical Parameters	27
4.1.8	VOF Tracer	28
4.2	Characterization of the problem and its code	28
4.2.1	Units	28
4.2.2	VOF Tracer variable and init fraction	29
4.2.3	Definition of the domain and its boundaries	29
4.2.4	Global Definitions	31
4.2.5	Output	31
4.2.6	Example script: c1.gfs	33
4.3	Volume of Fluid method	34
5	Additional Software	36
5.1	Data Process	36
6	Results	39
6.1	Constant profile	42
6.1.1	Simulation C1	43
6.1.2	Simulation C2	45
6.1.3	Simulation C3	48
6.1.4	Simulation C4	49
6.1.5	Simulation C5	50
6.2	Linear profile	52
6.2.1	Simulation L1	53
6.2.2	Simulation L2	56
6.2.3	Simulation L3	58
6.2.4	Simulation L4	60
6.2.5	Simulation L5	61

6.3	Parabolic profile	63
6.3.1	Simulation P1	64
6.3.2	Simulation P2	65
6.3.3	Simulation P3	68
6.3.4	Simulation P4	71
6.3.5	Simulation P5	72
7	Conclusions and future work	74
7.1	Conclusions	74
7.1.1	Normal distribution on small droplets	74
7.1.2	Number of droplets vs speed	75
7.1.3	Number of droplets vs dynamic viscosity	75
7.2	Future work	76
7.2.1	Computer's performance	76
7.2.2	More velocity profiles	76
A	Script for filtering first droplet of Gerris output file	77
B	Script for droplets characterization	78
C	Function for comparing vectors	80

List of Figures

2.1	Sketch of a hybrid rocket motor.	12
3.1	Instability of the layer of paraffin	17
3.2	Some paraffin kinds	18
4.1	Gerris lacustris	21
4.2	Refinement for n=3	24
4.3	Refinement for n=5	24
4.4	Refinement for n=6	24
4.5	Domain	29
4.6	Boundaries	30
5.1	Fragment of volume.dat	37
5.2	New Droplet	38
6.1	Constant Profile	42
6.2	Total droplets in C1	44
6.3	Droplets in C1 without biggest ones	44
6.4	Total droplets in C2	46
6.5	Droplets in C2 below $1.5 \cdot 10^{-7} m^3/m$	46
6.6	Droplets in C2 above $1.5 \cdot 10^{-7} m^3/m$	47
6.7	Total droplets in C4	49
6.8	Total droplets in C5	50

LIST OF FIGURES

6.9	Droplets in C5 below $1.5 \cdot 10^{-7} m^3/m$	51
6.10	Droplets in C5 above $1.5 \cdot 10^{-7} m^3/m$	51
6.11	Linear profile	52
6.12	Total droplets in L1	54
6.13	Droplets in L1 below $1.5 \cdot 10^{-7} m^3/m$	54
6.14	Droplets in L1 above $1.5 \cdot 10^{-7} m^3/m$	55
6.15	Total droplets in L2	56
6.16	Droplets in L2 below $1.5 \cdot 10^{-7} m^3/m$	57
6.17	Droplets in L2 above $1.5 \cdot 10^{-7} m^3/m$	57
6.18	Total droplets in L3	58
6.19	Droplets in L3 below $1.5 \cdot 10^{-7} m^3/m$	59
6.20	Total droplets in L5	61
6.21	Droplets in L5 below $1.5 \cdot 10^{-7} m^3/m$	62
6.22	Droplets in L5 above $1.5 \cdot 10^{-7} m^3/m$	62
6.23	Parabolic profile	63
6.24	Total droplets in P2	66
6.25	Droplets below $1.5e-7 m^2$ in P2	66
6.26	Droplets above $1.5e-7 m^2$ in P2	67
6.27	Total droplets in P3	69
6.28	Droplets below $1.5e-7 m^2$ in P3	69
6.29	Droplets above $1.5e-7 m^2$ in P3	70
6.30	Total droplets in P4	71
6.31	Total droplets in P5	72
6.32	Droplets below $1.5e-7 m^2$ in P5	73
6.33	Droplets above $1.5e-7 m^2$ in P5	73

List of Tables

3.1	Properties of paraffin wax evaluated at 533K	19
6.1	Simulation parameters for C1	43
6.2	Simulation results of C1	43
6.3	Simulation parameters for C2	45
6.4	Simulation results of C2	45
6.5	Simulation parameters for C3	48
6.6	Simulation results of C3	48
6.7	Simulation parameters for C4	49
6.8	Simulation results of C4	49
6.9	Simulation parameters for C5	50
6.10	Simulation results of C5	50
6.11	Simulation parameters for L1	53
6.12	Simulation results of L1	53
6.13	Simulation parameters for L2	56
6.14	Simulation results of L2	56
6.15	Simulation parameters for L3	58
6.16	Simulation results of L3	58
6.17	Simulation parameters for L4	60
6.18	Simulation results of L4	60
6.19	Simulation parameters for L5	61
6.20	Simulation results of L5	61

LIST OF TABLES

6.21	Simulation parameters for P1	64
6.22	Simulation results of P1	64
6.23	Simulation parameters for	65
6.24	Simulation results of P2	65
6.25	Simulation parameters for P3	68
6.26	Simulation results of P3	68
6.27	Simulation parameters for P4	71
6.28	Simulation results of P4	71
6.29	Simulation parameters for P5	72
6.30	Simulation results of P5	72
7.1	Linear profile comparison	75

Chapter 1

Introduction

This project is framed in the aerospace field, particularly with respect to the systems of propulsion. In this field, the object of this study is in hybrid propulsion understood as a particular case of chemical propulsion, extended within the scope of rockets.

One of the most influential parameters on performance of propellants of this type is the rate of regression of solid grain. In some cases, when the solid is, for example, paraffin, a film of liquid is formed between the solid and liquid airflow, and due to the airflow some droplets come off of this film.

The characterization of the drops of paraffin will be the main subject of the thesis.

1.1 Motivations

Nowadays, in the propulsion field, chemical ones are the most spread systems. Particularly the most used are solid and liquid propellants while historically those known as hybrid propellant haven't been properly developed. Then, it's been in these last years that they became the next line of investigation.

Hybrid rockets exhibit advantages over both liquid rockets and solid rockets especially in terms of simplicity, safety, and cost. Because it is nearly impossible

for the fuel and oxidizer to be mixed intimately (being different states of matter), hybrid rockets tend to fail more benignly than liquids or solids. Like liquid rockets and unlike solid rockets they can be shut down easily and are simply throttle-able.

At the present time, due to those advantages (and disadvantages), research into hybrid propulsion and its issues are at the forefront of the propulsion research activity.

1.2 Objectives

The aim of this thesis is to simulate the behavior of a given volume of liquid paraffin when hit by an air flow parallel to the surface of that volume. We are particularly interested in the number of drops that form, and size for a given period of time and according to different velocity profiles that might take the air flow.

To do this we use an open source software, called Gerris which operates especially well in Linux operating systems. It is a Free Software program for the solution of the partial differential equations describing fluid flow

Additionally developed Matlab routines for the handling of outputs that provides Gerris were developed.

1.3 Outline

Chapter 1

This chapter frames the work developed in the thesis in terms of motivations and objectives, with an explanation of the development of the thesis in the field of hybrid propulsion technology.

Chapter 2

In this part the importance of hybrid propulsion in these times is explored, the comparison with other types of chemical propulsion is performed and a brief

description of the operation of such engines is described.

Chapter 3

This and the next chapter present general characteristics of paraffins and their physical and chemical properties.

Chapter 4

The main aspects of Gerris, such as the characteristics of the code, its governing equations and the information gotten from it, are described in this chapter. Also an explanation about the Volume of Fluid method is given.

Chapter 5

Programs developed in Matlab, in order to process the incoming data from Gerris, are presented.

Chapter 6

Results of the simulations and data processing are presented and commented.

Chapter 7

Finally, conclusions obtained after the developed work, the analysis of the results and future improvements are describe in this final chapter.

Chapter 2

Hybrid Rocket Propulsion

2.1 Introduction

In its simplest form a hybrid rocket consists of a pressure vessel (tank) containing the liquid propellant, the combustion chamber containing the solid propellant, and a valve isolating the two. When thrust is desired, a suitable ignition source is introduced in the combustion chamber and the valve is opened. The liquid propellant (or gas) flows into the combustion chamber where it is vaporized and then reacted with the solid propellant. Combustion occurs in a boundary layer diffusion flame adjacent to the surface of the solid propellant. Generally the liquid propellant is the oxidizer and the solid propellant is the fuel because solid oxidizers are problematic and lower performing than liquid oxidizers. Furthermore, using a solid fuel such as HTPB or paraffin allows for the incorporation of high-energy fuel additives such as aluminium, lithium, or metal hydrides. Common oxidizers include gaseous or liquid oxygen or nitrous oxide. Common fuels include polymers such as polyethylene, cross-linked rubber such as HTPB or liquefying fuels such as paraffin.

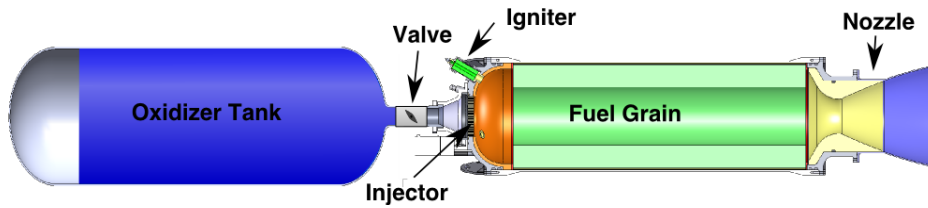


Figure 2.1: Sketch of a hybrid rocket motor.

2.2 A short summary about the history of hybrid rockets

The recent literature includes significant review papers [1–5], the scale effects analysis [6], the fuel characterization [7–10], methods to increase the regression rate [11]. Among these, some efforts deal with the influence on performance of the oxidizer injection system [12–14]. Two main research trends can be observed. The first concerns the use of nano metal powders, as ingredients able to increase the solid fuel regression rate. On this topic research activities were performed in Russia and at The Pennsylvania State University [4, 15, 16]; aluminium and boron powders, micro and nano-sized, were investigated. The second trend focuses on the use of paraffin-based solid fuels, also investigating the so-called entrainment phenomenon. On this topic the work made by Karabeyoglu and Cantwell at Stanford University is particularly meaningful [17–19]. The regression rate increase due to the introduction of aluminium particles, or of other energetic material, in the fuel grain dates back to 1965. Indeed, based on the heat transfer limited regression rate theoretical model, in comparison with the pure fuel, the regression rate increases proportionally to the metallic particles mass fraction [20, 21]. Some test performed with micro particles of aluminium have confirmed a non significant increasing in regression rate and a relevant aluminium residue in exhausts; this means that particles do not participate to the combustion process. Nowadays, due to the progresses in the field of nano-technology, the idea of dispersing aluminium nano-sized particles in the fuel seems a good proposal [22, 23]. The study of the gas flow evolution inside the motor is essential for the correct modeling of the flow/surface interactions and in particular for the estimation of the regression rate which determines the overall sizing, mass fluxes, and geometric configuration of the hybrid motor. Therefore, more comprehensive computational fluid dynamic (CFD) models based on a coupled fluid/structure analysis are necessary for improved design and predic-

tion capability. CFD codes weakly coupled with the models that describe the thermal behavior of the solid material [24] represent the first set of studies found in the open literature. However, to correctly evaluate the hybrid rocket engine behavior it is fundamental to study the complex coupling between CFD and fuel solid surface through a detailed description of the physico-chemical phenomena that occur at fluid-solid interface (as addressed in [25] for the ablative thermal protection materials). In addition for the modeling of the combustion processes, homogeneous chemical reactions simplified models are used [26, 27]. The complete numerical simulation of the flowfield inside hybrid motors requires adequate models both for the surface thermochemistry and for the homogeneous combustion. The most important and detailed results are the ones obtained by the Purdue University [26]. In this case the problem has been analyzed using a standard Navier-Stokes solver that includes the turbulent transport and chemical species equations, with a simplified kinetic model for the gaseous combustion process with 5 species and 2 global reactions involved [26, 27].

The solid fuel pyrolysis is modeled with an Arrhenius type expression. A detailed analysis through CFD can have a useful role in understanding the combustion process and hence in the design of combustion chambers in hybrid motors. Other studies have instead only faced the part which concerns the flow over ablative thermal protection systems (solid rocket motors, reentry vehicles). In particular, surface mass and energy balances have been introduced at the fluid-solid interface which become a boundary condition for the Navier-Stokes solver. Hybrid rocket motors are attractive as they present some of the benefit of both liquid rocket engines and solid rocket motors. Hybrid rocket motors can be shut-off and restarted like liquid rocket engines, and can be throttled within a wide thrust range. Moreover, special safety steps needed for chemicals such as NTO, MMH and UDMH are eliminated and operation costs fall as a result. A large number of papers concerning numerical and experimental investigations can be found in the literature [28–30].

2.3 Advantages and disadvantages of hybrid propulsion

2.3.1 Advantages compared with bipropellant liquid propulsion:

- Mechanically simpler: requires only a single liquid propellant resulting in less plumbing, fewer valves, and simpler operations.
- Denser fuels: fuels in the solid phase generally have higher density than those in the liquid phase, reducing overall system volume.
- Metal additives: reactive metals such as aluminum or magnesium, can be easily included in the fuel grain increasing specific impulse(I_{sp}), density specific impulse, or both.

2.3.2 Advantages compared with solid propulsion:

- Higher theoretical I_{sp} is possible.
- Less explosion hazard: propellant grain more tolerant of processing errors such as cracks.
- More controllable: start/stop/restart and throttling are all achievable with appropriate oxidizer control.
- Safe and non-toxic oxidizers such as liquid oxygen and nitrous oxide can be used.
- Can be transported to site in a benign form and loaded with oxidizer remotely immediately before launch, improving safety.

2.3.3 Disadvantages of hybrid propulsion:

Hybrid rockets also exhibit some disadvantages when compared with liquid and solid rockets. These include:

- Oxidizer-to-fuel ratio shift ("O/F shift"): with a constant oxidizer flow-rate, the ratio of fuel production rate to oxidizer flow rate will change as a grain

regresses. This leads to off-peak operation from a chemical performance point of view.

- Low regression-rate (rate at which the solid phase recedes) fuels often drive multi-port fuel grains. Multi-port fuel grains have poor volumetric efficiency and, often, structural deficiencies.

High regression-rate liquefying fuels developed in the late 1990s offer a potential solution to this problem. For a well-designed hybrid, O/F shift has a very small impact on performance because is insensitive to O/F shift near the peak.

In general, much less development work has been performed with hybrids than liquids or solids and it is likely that some of these disadvantages could be rectified through further investment in research and development.

Chapter 3

Properties of paraffin-based fuels

3.1 Liquefying hybrid fuels

In the late 1990s a new class of high regression rate paraffin-based fuels was discovered at Stanford University. The high regression rate of these fuels is due to a droplet entrainment mass transfer mechanism that adds to the conventional evaporation mass transfer. These fuels produce a very thin, low viscosity, low surface tension liquid layer on the fuel surface when they burn. The instability of this layer, illustrated in figure 3.1, is driven by the oxidizer gas flow in the port. Droplets of fuel lift-off and entrain in the gas stream, which greatly increases the overall fuel mass transfer rate. These fuels burn fast enough to enable desired thrust levels to be produced in a single port design. Note that not all fuels that form a melt layer at the fuel surface will entrain. For example, high-density polyethylene (HDPE), a conventional hybrid fuel, forms a melt layer that is too viscous to permit droplet entrainment.

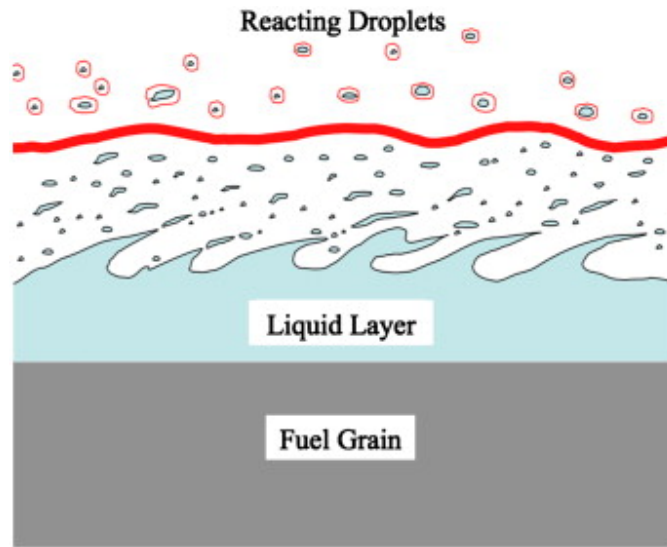


Figure 3.1: Instability of the layer of paraffin

The regression rates of paraffin-based fuels are generally from three to four times higher than conventional hybrid fuels (e.g. HTPB). At oxidizer mass fluxes typical of commercial applications, space-time averaged regression rates of up to 4.7 mm/s are measured for these fuels with a corresponding instantaneous regression rate at the beginning of burn of 8.4 mm/s. The fast burn rate allows for a simple single circular port grain design and results in significantly improved volumetric fuel loading and significantly increased fuel utilization (typically more than 97%).

This hybrid fuel also enjoys the added flexibility of having an adjustable regression rate. Slight alterations in additive concentration can change this rate by more than a factor of two. This is a critical virtue that can be quite beneficial in designing efficient hybrid systems with mission flexibility. Casting hybrid fuel grains is a relatively simple process that can be carried out at a small-scale facility. The fuel composition needed for a given mission including structural additives is melted and then cooled and solidified into the required grain size and shape using a centrifugal casting process designed to produce crack-free and void-free grains. No polymerization reactions are involved nor are curing agents required. The scrap pieces of fuel can be re-melted and reused. Because of its fundamental inertness, deterioration in storage is not an issue and its safe handling property is especially

important in shipping where no special precautions are needed, resulting in appreciable cost savings.

3.2 Paraffin wax

Wax is an organic, plastic-like substance that is solid at ambient temperature and becomes liquid when melted. Because wax is plastic in nature, it usually deforms under pressure without the application of heat.

The following summarizes the general features of wax:

- Solid at ambient temperature
- Thermoplastic in nature
- Combustible
- Liquid at 45 to 95°C
- Insoluble in water

The term "wax" is applied to a large number of chemically different materials. Technological advances in the world today have led to an increasing number of commercially available substances of various chemical compositions and properties which have acquired the name "wax". In the most general terms, waxes are "naturally" or "synthetically" derived.

Paraffin wax consists mostly of straight chain hydrocarbons with 80 to 90% normal paraffin content and the balance consists of branched paraffins (iso-paraffins) and cycloparaffins. In the figure 3.2 is shown three examples of paraffin.

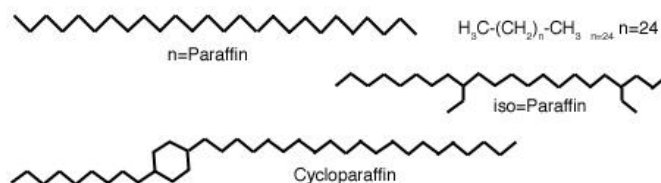


Figure 3.2: Some paraffin kinds

As said paraffin waxes are hydrophobic, making them an ideal binder for metal, metal hydride or dense organic additives (e.g. aluminum powder). This enables the hybrid to achieve a specific impulse (Isp) and density advantage over a comparable hydrocarbon-fueled liquid system. An important, but subtle, effect of aluminum addition to the fuel is that it tends to shift the combustion to a lower oxidizer to fuel (O/F) ratio. Therefore, for the same total propellant mass there is a larger proportion of the denser solid propellant. This reduces the tank size required for the liquid oxidizer and leads to a less massive system overall, thus producing a better-performing system.

In the Table 3.1 there is a summary of the main properties of the paraffin considered in the model of Gerris. The properties used has been surface tension, viscosity and density in the liquid Phase. This properties has been measured in the mean temperature between melting and vaporization temperature.

Property	Units	Value
Molecular weight	g/mol	432.8
Heat of formation	kJ/mol	-697.2
Surface tension	mN/m	7.1
Viscosity	mPa-s	0.65
Density-liquid phase	kg/m	654.4
Melting temperature	K	339.6
Boiling temperature	K	727.4
Heat of fusion	kJ/kg	167.2
Heat of vaporization	kJ/kg	163.5
Thermal conductivity, liquid phase	W/(m·K)	0.12
Specific heat, liquid phase	kJ/(kg·K)	2.92
Specific heat, solid phase	kJ/(kg·K)	2.03

Table 3.1: Properties of paraffin wax evaluated at 533K

Chapter 4

Gerris Model

The software used to solve the flow is called *Gerris Flow Solver (Gerris)*. It is a Freeware program for solving partial differential equations describing fluid flow. Specifically, it is a tree-based adaptive solver for the incompressible Euler equations in complex geometries. To deal with two-phase systems, *Gerris* uses a mathematical method known as *Volume of Fluid*, which is a numerical technique for tracking and locating the free surface (or fluid-fluid interface). It can solve both two-dimensional and three-dimensional problems. Only the two-dimensional feature has been utilized in this thesis.

Gerris also conceptualizes the interaction between a fluid and a defined solid object. This can be designed with an implicit formula within *Gerris* code or imported from other utilities such as CAD packages. However, files need to be in GTS format to be compatible with *Gerris*.

Gerris is a console-based program. When a parameter or simulation file is inputted, it can produce various output files. All elements needed to run the simulation is specified in the *Parameter File*, this includes:

- layout of the simulation domain
- initial conditions
- boundaries conditions

- solid boundaries
- what is outputted and when
- control parameters for the numerical schemes

The simulation file will be analyzed in the following section in this chapter and the output also will be analyzed in its corresponding section.

Finally, it is also worth mentioning the origin of the name Gerris. It refers to Gerris insects or 'Pond Skaters' shown in Figure 4.1. Due to hydrophobic characteristics of their legs, they take advantage of the surface tension of water to float as they move through the surface.



Figure 4.1: *Gerris lacustris*

4.1 General characteristics of the Gerris code

Gerris is a Partial Differential Equations Solver (PDES) for the time-dependent, incompressible and variable-density Euler, Stokes or Navier-Stokes equations. Gerris is also a programming language whose words, syntax and structure are discussed in this section.

The Gerris language is composed by words that reflect the internal structure of the code. The Gerriscode is written in C with inheritance. This means that the root of each word is a component of its parent.

For example the below commands have the same parent (`GfsOutput`), which write the simulation data:

- **GfsOutputTiming** (write a summary of the time usage of this simulation)
- **GfsOutputTime** (write the model time, *Time Step*, CPU time and real time)
- **GfsOutputSimulation** (write the whole simulation data)

In practice a code is written on a script line by following Gerris syntax and is interpreted by the Gerris solver.

4.1.1 The domain

Gerris builds a domain with 2 dimensional boxes or 3 dimensional cubes, whose sizes are unitary by default, but can be modified. The domain is defined by either the junction of several boxes/cubes or by using them individually. In this model, however, only the 2 dimensional boxes were used.

4.1.2 The boundary conditions

After the domain has been defined, the borders can be set. A box has 4 sides (top, bottom, left and right). The Gerris language uses keywords to define the boundary conditions.

By default, Gerris assumes that the boundaries are solid walls with no-slip conditions for the velocity

Gerris uses two families of words in this case: **GfsBoundary** and **GfsBc**, with the corresponding inheritances. **Gfsboundary** is used to define boundary conditions for the boxes using the following syntax:


```

1 GfsBoundary{
2   [GfsBc]
3   [GfsBc]
4 }

```

Where [GfsBc] is one of the following descendants:

- **GfsBcDirichlet** — Dirichlet boundary condition (i.e. value)
- **GfsBcNeumann** — Neumann boundary condition (i.e. value of the normal derivate)
- **GfsBcNavier** — Navier slip/Robin boundary condition

GfsBoundary also has two descendants:

- **GfsBoundaryInflowConstant** — Constant inflow
- **GfsBoundaryOutflow** — Free outflow

4.1.3 The refinement

There are two types of refinements made here.

Firstly, the *initial refinement*, is carried out by the command **Refine**, which is always followed by an integer that is the exponent **n** in the following equation:

$$\text{Number of cells} = 2^n$$

This type of refinement shows the number of cells there are in the mes, for each box.

For example, if the command line is '**Refine 5**' (i.e. $n=5$), the mesh for one box will be: $2^5 = 32$ cells.

In the figures 4.2, 4.3 and 4.4 the meshes for $n=3, 5, 6$ are respectively shown.

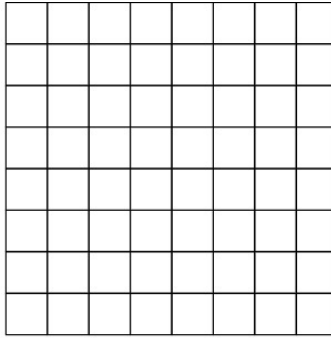


Figure 4.2: Refinement for $n=3$

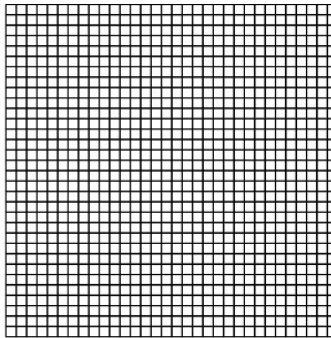


Figure 4.3: Refinement for $n=5$

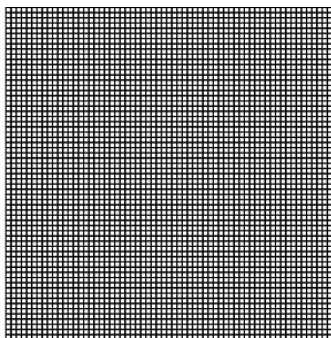


Figure 4.4: Refinement for $n=6$

Secondly, the other type of refinement refers to the adaptive meshing that occurs from the second *Time Step* of the computer. The quadtree structure of the discretization is used to adaptively follow the small structures of the flow, allowing

the program to focus on the area where it is most needed.

This is done using **GfsAdapt**. Various criteria can be used to determine where a refinement is needed. **GfsAdapt** is the base class for the objects to dynamically adapt, the parameters are:

- **minlevel** — The minimum number of refinement levels (default is 0)
- **maxlevel** — The maximum number of refinement levels (default is infinite)
- **mincells** — The minimum number of cells in the simulation (default is 0)
- **maxcells** — The maximum number of cells in the simulation. If this number is reached, the algorithm optimizes the distribution of the cells so that the maximum cost to the cells is minimized (default is infinite)
- **cmax** — The maximum cell cost allowed. The cell will be refined if the number of cells is smaller than the maximum allowed, and the cost of a cell is larger than this value.
- **weight** — When combining several criteria, the algorithm will 'weight' the cost of each criteria by this value in order to work out the total cost (default is 1)
- **cfactor** — Cells will only be processed if their cost is smaller than **cmax** or **cfactor** (default is 4)

One particular inheritor is noteworthy, **GfsAdaptGradient**, is used to adapt cells depending on the local gradient of a variable. It has been widely used through out this thesis as it is useful to study interfaces. The variable is one which defines the volume of fluid that passes from 1 to 0 from either side of the interface.

4.1.4 The time

GfsTime defines the starting and finishing time for the run, either in terms of floating-point model time, the integer time-step or a combination of both.

In the case studied, the time setup is long enough to carry out the whole simulation until the convergence error is reached, and the simulation stops itself. Note also that the overall simulation is only stable for CFL number smaller than 0.5 ($C_{\max} = 0.5$)

The CFL number is given by:

$$C = \frac{u_x \Delta t}{\Delta x} + \frac{u_y \Delta t}{\Delta y} < C_{\max} \quad (4.1)$$

4.1.5 The output of the code

Gerris comes with objects that allow the output of specific simulation data.

The parent of **GfsOutput** is **GfsEvent**. This is used to control any action to be performed at any given time during a simulation. This includes one-off actions as well as periodically repeated actions.

Children of **GfsOutput** are specially useful for the purposes of this study:

- **GfsOutputTime** — displays the model time, *Time Step*, CPU and real time while the simulation is running
- **GfsOutputLocation** — writes the values of all permanent variables at a set of given locations. This is useful when establishing the interpolated profile.
- **GfsOutputSimulation** — writes a description of the current state of the simulation which contains the standard simulation parameters, layout of the cell hierarchy and associated variable values. In combination with some commands in Linux, the option to show parameters while the simulation is running at the current *Time* is available.
- **GfsOutputDropletSum** — one of the most relevant commands in order to measure the droplets. It outputs a file containing a matrix with three columns. Each row identifies a droplet. In the first column the Time Step is shown. The second contains an Identifier that numbers the droplets from the highest to the lowest volume which share the same Time Step. The last column shows the volume of the droplet.

- **GfsOutputPPM** — shows a colour image of the given scalar field in PPM. If the chosen scalar field is the VOF variable, it shows the evolution of the system through time.

4.1.6 Initial Conditions

For defining initial conditions such as the fraction of liquid and gas, or the initial velocities, the command **Init** and its child **InitFraction** are used respectively.

4.1.7 Physical Parameters

The physical parameters of the fluids necessary to define the problem are the density and viscosity of both phases, and the surface tension between them.

For the density the command **PhysicalParams** is used. **Alpha** is used as the reciprocal of the density.

The viscosity uses the command **SourceViscosity**, followed by its value.

Lastly, for defining the the surface tension two commands are needed. The **Gfs-VariableCurvature** contains the mean curvature of an interface defined through a *VOF Tracer*. Its syntax is

```
1 GfsVariableCurvature variable-of-curvature variable-of-tracer
```

Once the variable-of-curvature is defined the surface tension can be set as:

```
1 GfsSourceTension variable-of-tracer value-of-surface-tension
   variable-of-curvature
```

4.1.8 VOF Tracer

Gerris uses a VOF (Volume of Fluid) technique to follow interfaces. The VOF is a numerical technique for tracking and locating interfaces, in particular fluid-fluid interfaces.

Gerris first defines the marker of the interface using `GfsVariableTracerVOF`, which defines a volume- fraction field advected ??? using the geometrical VOF technique.

The tracer will be advected, and will need to define the geometrical position of the boundary. To define the frontier, Gerris uses the command `GfsInitFraction` (explained previously) using a function of implies surface.

4.2 Characterization of the problem and its code

After the main features of Gerris has been explained, the problem of the flow of gas parallel to film of paraffin wax will be applied as shown in the example code at the end of the section (in the subsection 4.2.6).

4.2.1 Units

There are two ways to undertake the dimensional problem. Firstly, a dimensionless way of treating the problem where the length would be unitary. However, the only relevant parameters would be the Reynold number selected as the reciprocal of the dynamic viscosity and the velocity. The second way involves the problem being fully dimensioned. Since Gerris has no units, it is important to make sure the units are chosen ccongruently, i.e. if the meter is selected as distance $Pa \cdot s$ must be selected as dynamic viscosity instead of cPs . The parameters are the SI (International System of Units), therefore:

- length: meters
- velocity: meters /second
- viscosity: pascal second

- density: kilograms / meters³
- surface tension: newton / meter

4.2.2 VOF Tracer variable and init fraction

The value of the VOF Tracer variable, in this instance named **T**, determines whether the content of a cells is liquid or gas. When the **T** value is 1, it corresponds to a liquid cell and when the **T** value is 0 it is gas. For a consistent definition of the tracer, the interface values must also be set. These definitions are given in lines 16 and 17 of code.

4.2.3 Definition of the domain and its boundaries

As can be seen in the figure 4.5 the domain is composed by 6 boxes, numbered from 1 to 6. In the first line of the code the number of boxes is set. The last seven lines of code specifies how the boxes connect to each other. For example, '1 2 right' refers to box 1 being connected to the box 2 via its right border.

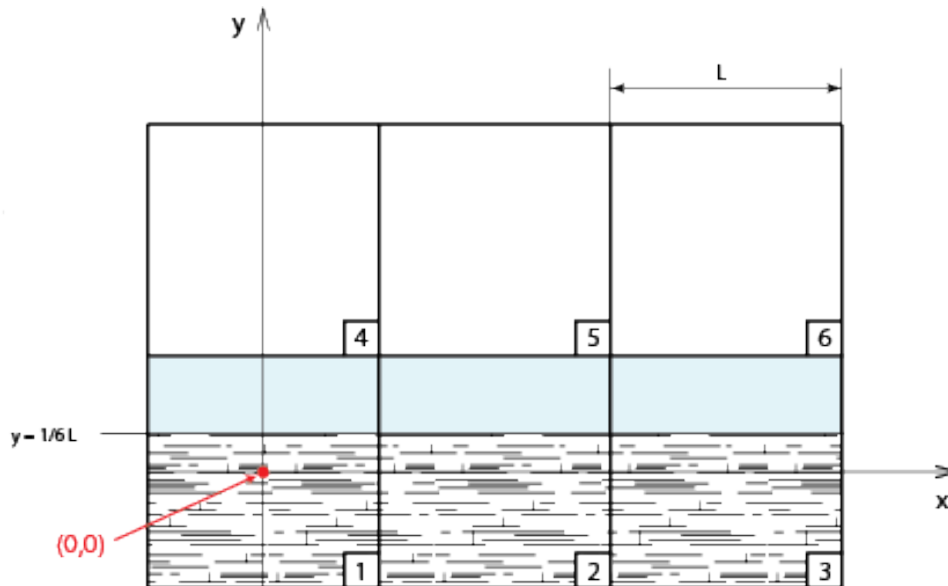


Figure 4.5: Domain

The frame of reference is a Cartesian coordinate system that has its origin in

the center of the first box.

'L' would be the length of the single box, named in the script file as *length*, and its value is 3.5 cm. It has been defined as a solid under $y=1/6 L$, which represents the paraffin which has not been melted yet. There is another layer of liquid paraffin only present in the beginning, in the boxes 1, 2 and 3. Boxes 4, 5 and 6 is only present the gaseous phase initially.

With regards to the boundaries, figure 4.6 represents the borders with the corresponding bound condition. For solids, no conditions are imposed. For the boxes 1 and 6, Dirichlet conditions are imposed for liquid and gas profiles. Non-slip conditions are set at the top of the boxes 4, 5 and 6. Finally, an exit is indicated in the right borders, identified by Gerris as *Boundary Outflow*.

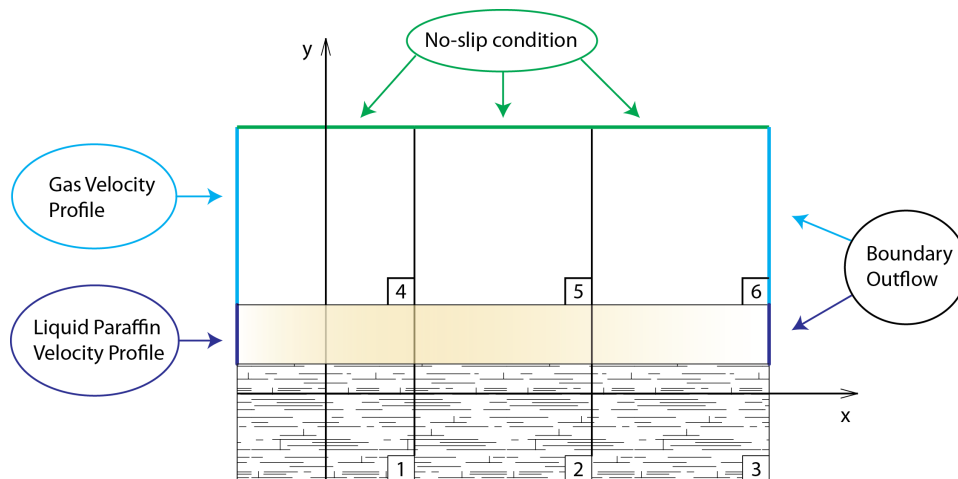


Figure 4.6: Boundaries

In the Gerris file, the above is written in the lines 36 to 54. Each *GfsBox* contains all the information related to its boundaries. This must be filled in order from the first (box 1), to the last (box 6). A special condition, however, is met in box 6. Beneath the velocity profile, there is another Dirichlet condition. This is associated to the VOF variable *T*. It has a value of zero, meaning that gas can only get in through that border. Without this condition, errors that lead to instability appear when a droplet goes backwards to that border.

4.2.4 Global Definitions

A set of variables are defined in the lines between 2 and 15. This has been done to make the file more manageable from one condition to the next. These variables will be analyzed in the following lines

- *level* corresponds to the maximum number of refinement levels.
- *rho_l* and *rho_g* are the densities of the paraffin and the air respectively. *rho(T)* is the function that gives *rho_l* when the tracer value is 1, and *rho_g* when the tracer value is 0. All units are SI values.
- *surft* is the surface tension between liquid paraffin wax and air
- Same as the density, the dynamic viscosities are also defined. *nu_l* and *nu_g* are the viscosities of paraffin and air, and *nu(T)* gives the value as a function of the Tracer - giving *nu_l* if T is 1, and *nu_g* if T is 0.
- *length* will be used to set the dimensions of the boxes.
- Assuming that liquid always has a linear profile, *U_l_max* is the maximum speed of the liquid which has reached the upper layer. *U_l(y)* is the velocity profile for the liquid, assumed zero in correlation with the solid wax layer.
- Finally, *U_l(y)* is another function which defines the air profile, in this case, constant.

once all these variables are defined, they can be used without any problems and the values cab changed in different simulations.

4.2.5 Output

In lines 30 to 34, there are two kinds of outputs. The three first lines cause Gerris to output the statistics of the simulation while it is running. The statistics include the current time, the convergence and a visual display of what is occurring.

In line 33, Gerris is outputting images to a ppm file that can later be converted to a mpg file.

In line 34, the droplets and its volume are recorded for each *Time Step*. This data will be explained in the next Chapter.

4.2.6 Example script: c1.gfs

```

1 6 7 GfsSimulation GfsBox GfsGEdge{}{
2   Global{
3     #define level 8
4     #define rho_l 654
5     #define rho_g 1.225
6     #define rho(T) ( T * rho_l + (1-T) * rho_g )
7     #define surf_t 0.0071
8     #define nu_l 0.00065
9     #define nu_g 0.0000178
10    #define nu(T) ( T * nu_l + (1-T) * nu_g )
11    #define length 0.035
12    #define U_l_max 0.005
13    #define U_l(y) (U_l_max*(3*y/length - 0.5))
14    #define U_g(y) 4
15  }
16  VariableTracerVOF T
17  InitFraction T (-1*(y-0.5*length))
18  Init {} {
19    U = ( T > 0.5 ? U_l(y) : U_g(y))
20    V = 0
21  }
22  GfsSolid(y-0.1666*length)
23  Refine 5
24  AdaptGradient { istep = 1 } { maxlevel = level cmax = 5e-2 } T
25  PhysicalParams { alpha = 1./rho(T) L = length}
26  VariableCurvature K T Kmax
27  SourceTension T surf_t K
28  SourceViscosity nu(T)
29  Time { end=2}
30  OutputSimulation { step = 0.001 } stdout
31  OutputTime { istep = 10 } stderr
32  OutputProjectionStats { istep = 10 } stderr
33  OutputPPM { step = 0.0003 } model_refine.ppm {v=T}
34  OutputDropletSums { istep = 1 } volume_refine.dat { v = T * dV}
35    T
36  }
37  GfsBox{
38    left = Boundary{
39      BcDirichlet U ( y > 0.16666*length && y < 0.5*length ? U_l(y):0)
40    }

```

```

40 }
41 GfsBox{}
42 GfsBox{
43     right = BoundaryOutflow
44 }
45 GfsBox{
46     right = BoundaryOutflow
47 }
48 GfsBox{}
49 GfsBox{
50     left = Boundary{
51         BcDirichlet U U_g(y)
52         BcDirichlet T 0
53     }
54 }
55 1 2 right
56 2 3 right
57 3 4 top
58 4 5 left
59 5 6 left
60 6 1 bottom
61 5 2 bottom

```

c1.gfs

4.3 Volume of Fluid method

In computational fluid dynamics, the volume of fluid method (or in short VOF method) is a numerical technique for tracking and locating the free surface (or fluid-fluid interface). It belongs to the class of Eulerian methods which are characterized by a mesh that is either stationary or is moving in a certain prescribed manner to accommodate the evolving shape of the interface. As such, VOF is an advection scheme a numerical recipe that allows the programmer to track the shape and position of the interface, but it is not a standalone flow solving algorithm. The Navier-Stokes equations describing the motion of the flow have to be solved separately. The same applies for all other advection algorithms.

The method is based on the idea of so-called fraction function C . It is defined as

the integral of fluid's characteristic function in the control volume (namely, volume of a computational grid cell). Basically, when the cell is empty, with no traced fluid inside, the value of C is zero; when the cell is full $C = 1$; and when the interphasal interface cuts the cell, then $0 < C < 1$. C is a discontinuous function, its value jumps from 0 to 1 when the argument moves into interior of traced phase.

The fraction function C is a scalar function, and while the fluid moves with velocity $\mathbf{v} = (u(x, y, z), v(x, y, z), w(x, y, z))$ (in three-dimensional space \mathbb{R}^3) every fluid particle retains its identity, i.e. when a particle is a given phase, it doesn't change the phase - like a particle of air, that is a part of air bubble in water remains air particle, regardless of the bubble movement (actually, for this to hold, we have to disregard processes such as dissolving of air in water). If that is so, then the substantial derivative of fraction function C needs to be equal to zero:

$$\frac{\partial C}{\partial t} + \mathbf{v} \cdot \nabla C = 0$$

This is actually the same equation that has to be fulfilled by the level set distance function Φ .

This equation cannot be easily solved directly, since C is discontinuous, but such attempts have been performed. But the most popular approach to the equation is the so called geometrical reconstruction, originating in the works of Hirt and B. D. Nichols.

The VOF method is known for its ability to conserve the "mass" of the traced fluid, also, when fluid interface changes its topology, this change is traced easily, so the interfaces can for example join, or break apart.

Chapter 5

Additional Software

Gerris was not the only software used in the development of the thesis. Matlab has also been used as a supporting tool to process the data from Gerris, characterize the droplets and to determine the coefficients of the approximate curve for the velocity profile via interpolation.

5.1 Data Process

The output file *volume.dat* (figure 5.1) gives for each *Time Step* a list of all the pieces of paraffin present in the control volume. This list consists of *Identifiers* associated with the value of the *Volume* (which is a *Surface* since the model is two-dimensional) for each piece and it is ordered from highest to lowest volume

At this point, there are several obstacles.

Firstly, the main volume of paraffin (reservoir) is always present in the list as the first element for a given *Time Step*. It would be tedious to keep the reservoir while writing the subsequent drop characterization scripts and would add extra time when carrying out the calculations through Matlab. To avoid this obstacle and to simplify calculations, the data file is filtered by removing the first row of each *Time step*, and re-numbering the *Identifiers*. This script is called *drop_filter.m* and it is included in the appendix

Time step	Identifier	Volume
0.266818	1	0.999841573458
0.266818	2	3.78693953017e-05
0.266818	3	3.76136657173e-05
0.266818	4	2.87063067146e-05
0.266818	5	1.47747361883e-06
0.267273	1	0.999840903351
0.267273	2	3.7869385755e-05
0.267273	3	3.76137292313e-05
0.267273	4	2.87050469742e-05
0.267273	5	1.47748107283e-06
0.267727	1	0.999840265328
0.267727	2	3.78680630007e-05
0.267727	3	3.76172489251e-05
0.267727	4	2.87064850111e-05
0.267727	5	1.47749021455e-06
0.268182	1	0.999839689445
0.268182	2	3.78691871337e-05
0.268182	3	3.76178134533e-05
0.268182	4	2.87064662105e-05
0.268182	5	1.47749063399e-06

Figure 5.1: Fragment of volume.dat

Additionally, *Identifiers* can be used for counting the drops at each time, however, they do not define each drop unequivocally in different *Time steps*. In order to count the drops generated and measure their size, it has been created another script (*droplets.m*). This script compares an array containing the volumes of the drops in the current time with another array containing the volumes in a previous time. This results in a third array containing the drops present in the current time which were not in the previous time. With this third array the creation of new drops can be measured (in the figure 5.2 the third array has just one element).

Included are two obvious limitations. Firstly, it is not known if a drop is formed from another drop, from the merger of two drops or directly from the reservoir of paraffin. And secondly, there is an error in the cases where at the same *Time step* a droplet is generated while another droplet either leaves the control volume, merges

Time Step 1	0.213583	1	0.999966537343	Array 1
	0.213583	2	3.7818625008e-05	
	0.213583	3	1.47721548952e-06	
Time Step 2	0.213984	1	0.999929392135	Array 2
	0.213984	2	3.78327978093e-05	
	0.213984	3	3.69761418107e-05	
	0.213984	4	1.47726820188e-06	
			Array 3	

Figure 5.2: New Droplet

with another drop or merges with the reservoir, and both of them have the size.

Chapter 6

Results

At this point, once the whole methodology has been exposed, the results will be present.

Three different velocities profiles have been studied: constant, linear and parabolic. All of them have 5 subcases with variation of the mean speed (scaling the whole profile) and variation of the viscosity (i.e. the temperature).

The velocity profiles are imposed in two different ways:

1. As inflow boundary condition — how the two different fluids enter the domain.
2. As initial condition — how were the fluids when the simulation started. This second kind is also very important as to reach good results this velocity profiles should be, as much as possible, similar to the velocity profiles the fluids would have after the transient had passed. Gerris makes fewer calculations in this case than in the case that both fluids depart from a motionless state.

The mathematical description of the velocity profiles are within the preamble in the definitions of Global Variables, so that when it changes from case to case, only there has to be modified.

The imposition of the profile are set in two different ways for each kind off condition:

1. As inflow boundary condition it is very intuitive as the only task is to put it as Boundary Condition on the left side of the boxes #1 and #6. For example:

```

1 #6
2 GfsBox {
3   left = Boundary {
4     BcDirichlet U U_g(y)
5   }

```

2. In the case of imposition of initial conditions, it has been wanted to assign the velocity profile to fluids rather than to space coordinates, so that this code has been used:

```

1 Init {} {
2   U = ( T > 0.5 ? U_l(y) : U_g(y) )
3 }

```

where $T > 0.5$ ($T = 1$) there is liquid so then $U_l(y)$ it's been used and where $T < 0.5$ ($T = 0$) there is gas so is been set to $U_g(y)$.

Liquid Velocity Profile

[figure] It's been supposed a Couette flow for the liquid phase. It is the result of integrating the Navier-Stokes equation from:

$$\frac{d^2U}{dy^2} = 0$$

where:

$U \equiv$ Velocity distribution

$y \equiv$ spatial coordinate

integrated for:

- $U_l(0.16667 \cdot L) = 0$ — No slip condition where the bottom plate is.
- $U_l(0.5 \cdot L) = U_{l,max}$ — Imposition of the speed on the interface. This $U_{l,max}$ will be different from the speed imposed to the gas in the same value spatial coordinate $y = 0.5L$ (in the interface) so that the entrainment phenomena appear.

As the system has been dimensioned to L (which value has been taken as 0.035m) also the spatial values have to be dimensioned to L .

Considering all this, the subsequent equation has been used to describe the liquid motion:

$$U_L(y) = U_{LMAX} \left(\frac{3y}{L} - 0.5 \right)$$

6.1 Constant profile

The constant profile has been the first to be tested. It's the simplest profile, and it has been simulated at different speeds in the cases C1, C2 and C3, starting with 4 m/s which is the minimum speed at which the formation of droplets process is meaningful. Then at C2 the speed has been increased to study its effect. Finally, C3 shows a simulation at a lower speed just to let know that the phenomenon is not important at all.

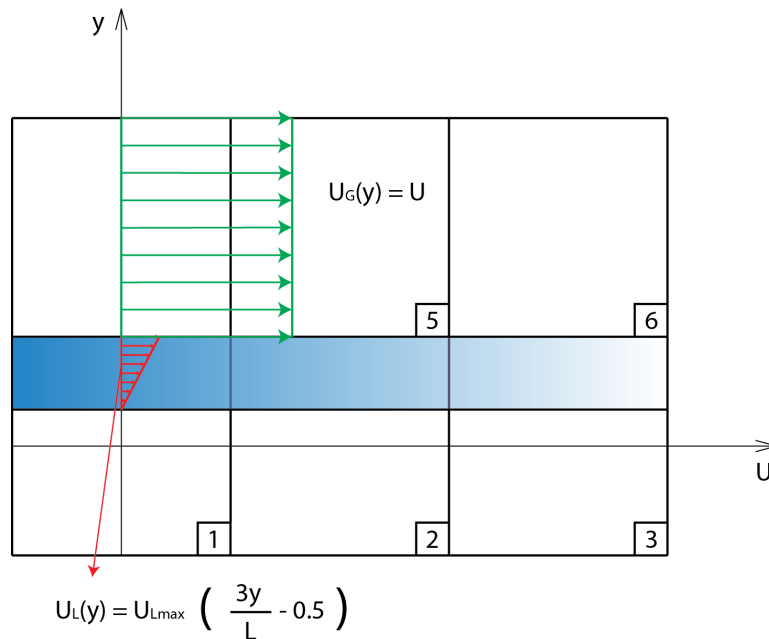


Figure 6.1: Constant Profile

With regard to simulations C4 and C5, they have the same speed as C2, but the dynamic viscosities change, being higher in the case of C4 and lower in the case of C5. This aims to simulate the experiment at different temperatures since there is a bound between temperature and dynamic viscosity.

For presenting the results has been chosen a set of three elements: a table with the simulation parameters, a table with the numeric results and a graphic in which the X axis represents the volume in cubic meters drops and the Y axis the amount of droplets with that volume. The number of figures could change in cases where

giving more information is needed or not even have a figure in the cases that there are very few droplets.

6.1.1 Simulation C1

Profile	Constant
Average Speed (m/s)	4
Viscosity ($Pa \cdot s$)	$0.65 \cdot 10^{-3}$
Simulation file	C1.gfs
Video file	C1.mpg

Table 6.1: Simulation parameters for C1

Time (s)	Total droplets	Volume detached (m^3/m)	Average droplet size (m^3/m)
0.05	619	2.4480e-05	3.9548e-05

Table 6.2: Simulation results of C1

These are the results obtained from the first simulation. In the figure 6.2 every droplet is considered. But due to a very low number of "big droplets" (who could be taken as singularities) the representation of the medium ones doesn't fit a normal distribution, so in order to show its similarity with gaussian curve, it has been illustrated in the figure 6.3 the same graphic just getting rid of the biggest droplets and re-adjusting the values on X axis. As a result of it, the distribution looks like more as the gaussian distribution.

The simulation video goes a bit further in time, but to compare with other simulations (which couldn't go further because of the limitation of Gerris, the computer performance characteristics or both of them) the results have been measured at the time of 0.05 seconds.

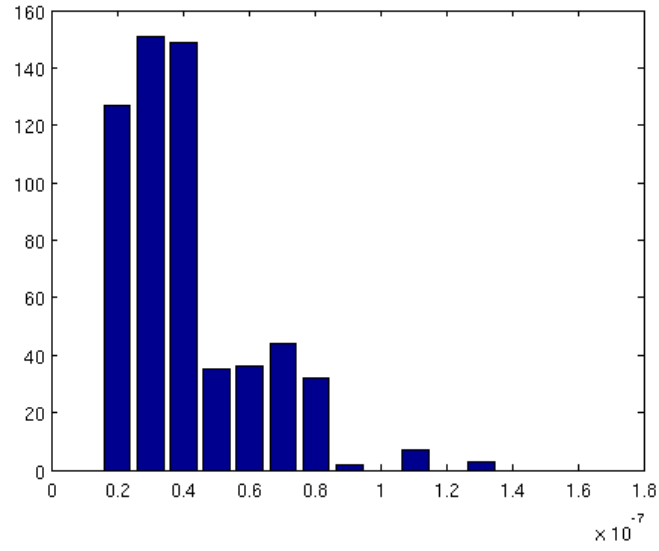


Figure 6.2: Total droplets in C1

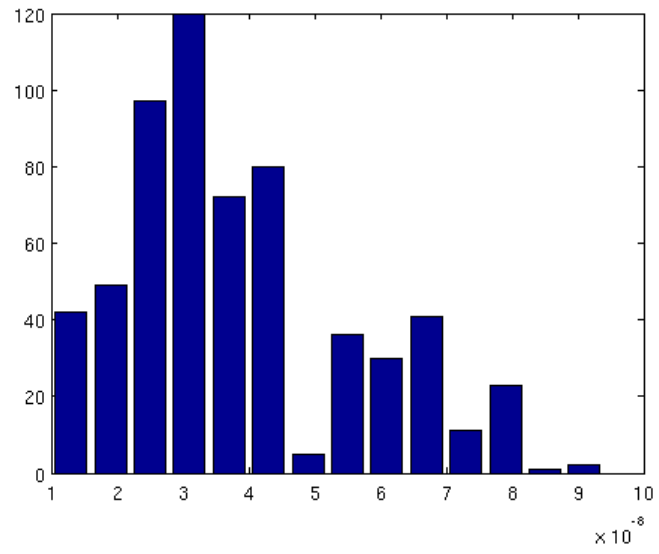


Figure 6.3: Droplets in C1 without biggest ones

6.1.2 Simulation C2

Profile	Constant
Average Speed (m/s)	7
Viscosity ($Pa \cdot s$)	$0.65 \cdot 10^{-3}$
Simulation file	C2.gfs
Video file	C2.mpg

Table 6.3: Simulation parameters for C2

Time (s)	Total droplets	Volume detached (m^3/m)	Average droplet size (m^3/m)
0.05	3149	3.3065e-04	4.8580e-08

Table 6.4: Simulation results of C2

The speed has been increased from 4 to 7 m/s . This has meant an increment about 400% in droplets and about 12 times more in volume detached. Then, it can be concluded that the speed module is a very relevant parameter. In this case also has been illustrated the whole size spectrum (Figure 6.4) followed by two more figures. Two trends can be observed. In the figure 6.5, the droplets whose volumes are smaller than $1.5 \cdot 10^{-7} m^3/m$ and in the figure 6.6 those one whose volume are greater than $1.5 \cdot 10^{-7} m^3/m$.

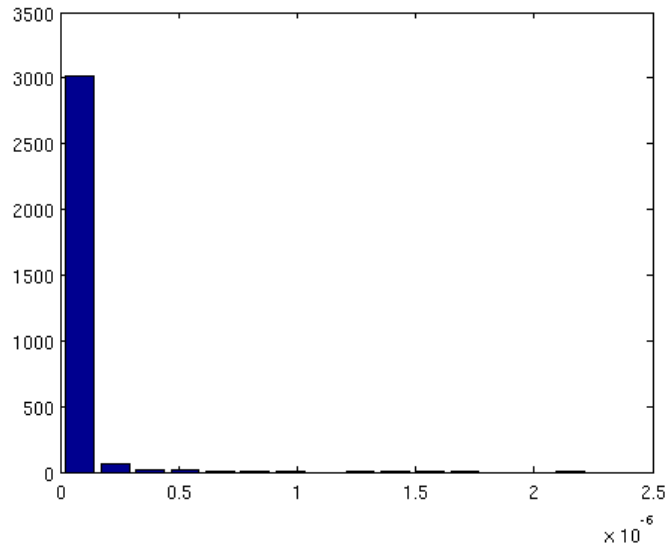


Figure 6.4: Total droplets in C2

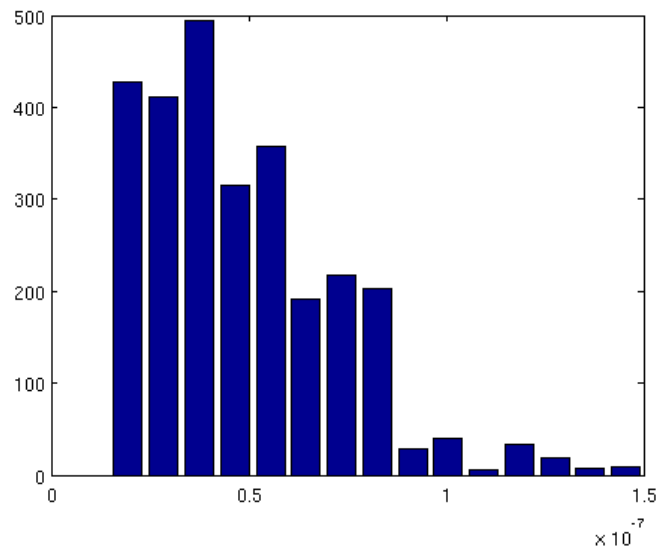


Figure 6.5: Droplets in C2 below $1.5 \cdot 10^{-7} m^3/m$

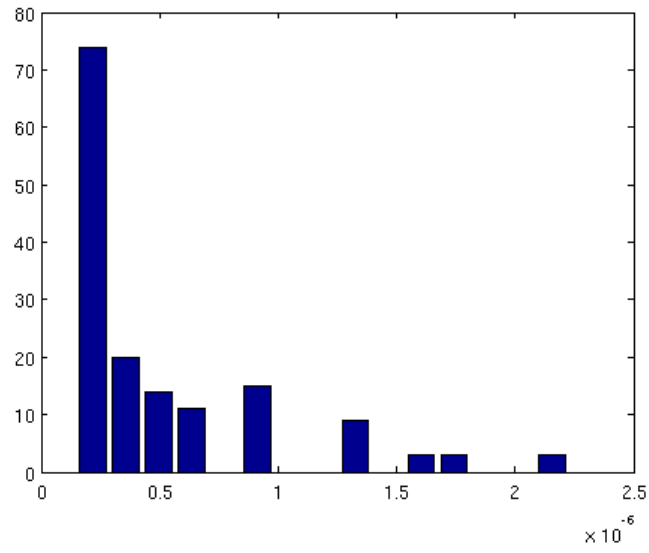


Figure 6.6: Droplets in C2 above $1.5 \cdot 10^{-7} m^3/m$

6.1.3 Simulation C3

Profile	Constant
Average Speed (m/s)	3
Viscosity ($Pa \cdot s$)	$0.65 \cdot 10^{-3}$
Simulation file	C3.gfs
Video file	C3.mpg

Table 6.5: Simulation parameters for C3

Time (s)	Total droplets	Volume detached (m^3/m)
0.05	4	$\equiv 0$

Table 6.6: Simulation results of C3

Only 4 droplets are formed. Therefore no figure is shown. The evolution of the system through the time can be followed in the video file. It can be concluded at this point that the number of droplets formed with this profile is very sensitive to the speed. As the speed increases also the detached volume does.

6.1.4 Simulation C4

Profile	Constant
Average Speed (m/s)	4
Viscosity ($Pa \cdot s$)	0.0034
Simulation file	C4.gfs
Video file	C4.mpg

Table 6.7: Simulation parameters for C4

Time (s)	Total droplets	Volume detached (m^3/m)	Average droplet size (m^3/m)
0.05	639	2.6511e-05	4.1488e-08

Table 6.8: Simulation results of C4

In this case the velocity is the same as in the case C1. This time the changing parameter has been the viscosity which has been increased from $0.00065 Pa \cdot s$ to $0.0034 Pa \cdot s$. The most remarkable fact is the huge decrease the entrainment phenomenon has suffered, from the 3149 droplets in C1 to 639 in C4. This was expected since the lower the temperature the nearer to solid state, so less droplets are formed.

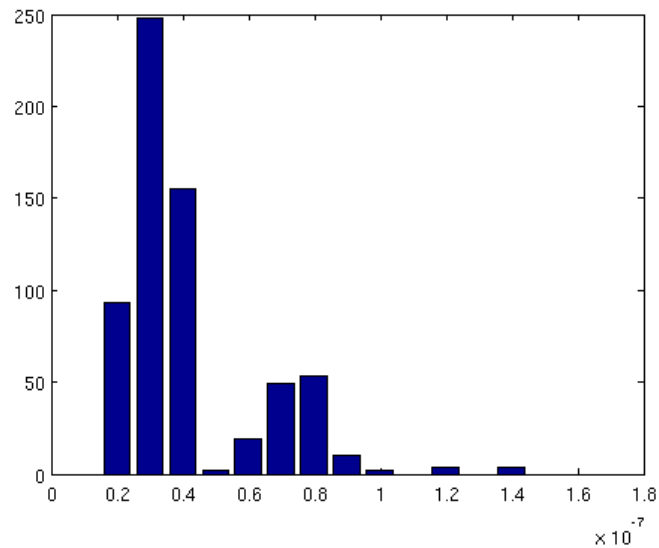


Figure 6.7: Total droplets in C4

6.1.5 Simulation C5

Profile	Constant
Average Speed (m/s)	4
Viscosity ($Pa \cdot s$)	0.000239
Simulation file	C5.gfs
Video file	C5.mpg

Table 6.9: Simulation parameters for C5

With same velocity as C2 and C4, simulation C5 has been carried out. The parameter which changes is the viscosity, this time lower than the case C2. Surprisingly, also this time the number of droplet has decreased which could mean that there is an optimal value of the viscosity between 0.000239 and 0.0034 $Pa \cdot s$.

Time (s)	Total droplets	Volume detached (m^3/m)	Average droplet size (m^3/m)
0.05	1955	9.8988e-05	4.8044e-08

Table 6.10: Simulation results of C5

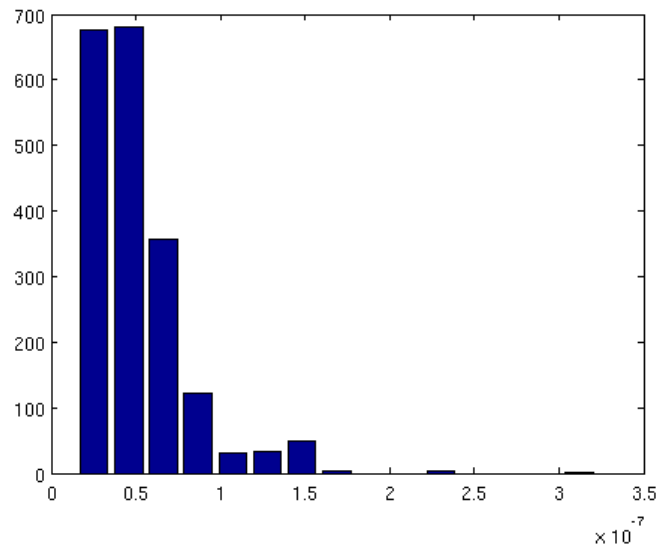


Figure 6.8: Total droplets in C5

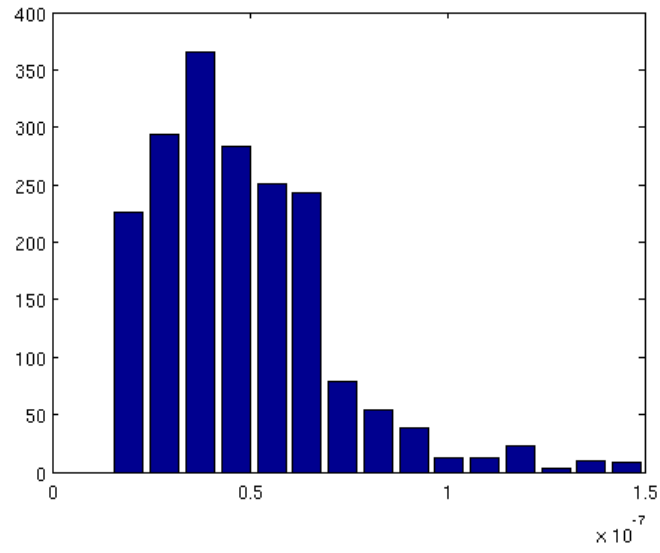


Figure 6.9: Droplets in C5 below $1.5 \cdot 10^{-7} m^3/m$

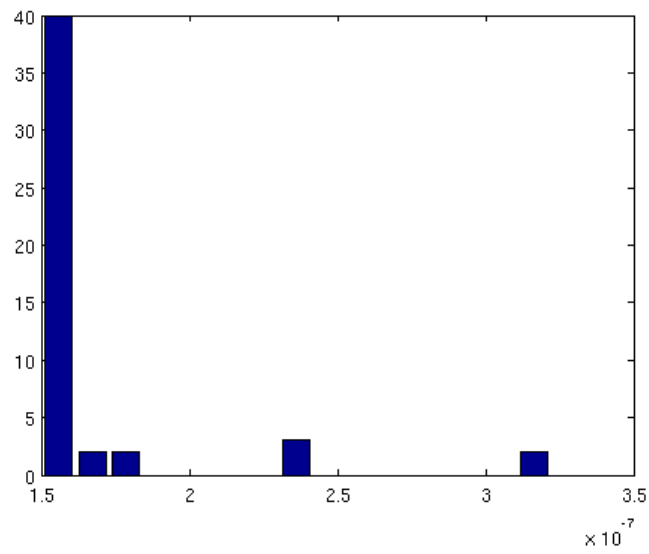


Figure 6.10: Droplets in C5 above $1.5 \cdot 10^{-7} m^3/m$

6.2 Linear profile

The line has been built from its generic formula $U = Ay + b$

The average speed (\bar{U} in the figure 6.11) has been imposed in $y = 1 \cdot L$ and zero speed in $y = 0 \cdot L$. This is:

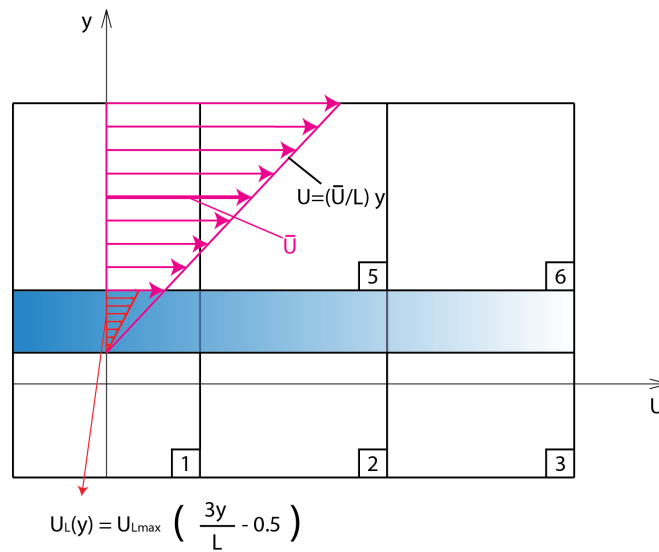


Figure 6.11: Linear profile

$$U = Ay + b$$

with:

$$U(1 \cdot L) = \bar{U}$$

$$U(0 \cdot L) = 0$$

so the resulting formula used in the linear profile is:

$$U = \frac{\bar{U}}{L}y$$

This way, in the interface there is a non zero speed, which seems an essential condition in order to reach the entrainment phenomenon. Other five simulations have been carried out. In the first three, average speed is the only parameter that varies. It takes for L1, L2 and L3 the values of 7, 9 and 6 m/s. Then taking L2

as reference, the values of the viscosity has been changed to a greater and a lower value in the simulations L4 and L5.

6.2.1 Simulation L1

Profile	Linear
Average Speed (m/s)	7
Viscosity ($Pa \cdot s$)	$0.65 \cdot 10^{-3}$
Simulation file	L1.gfs
Video file	L1.mpg

Table 6.11: Simulation parameters for L1

Time (s)	Total droplets	Volume detached (m^3/m)	Average droplet size (m^3/m)
0.03	941	6.3124e-05	4.9218e-08

Table 6.12: Simulation results of L1

With the same average speed as the case C2, the number of droplets withdrawn from the paraffin is much less (from 3149 to 941). A likely reason could be that even is the average speed is the same, in correspondence with the interface, L1 is the half than C2 ($3.5 m/s$). In fact is more similar to the case C1 (619 droplets).

Three figures are shown for this profile. The first with every single droplet, and the other two with small and big droplets (smaller and greater than $1.5e-07 m^3/m$).

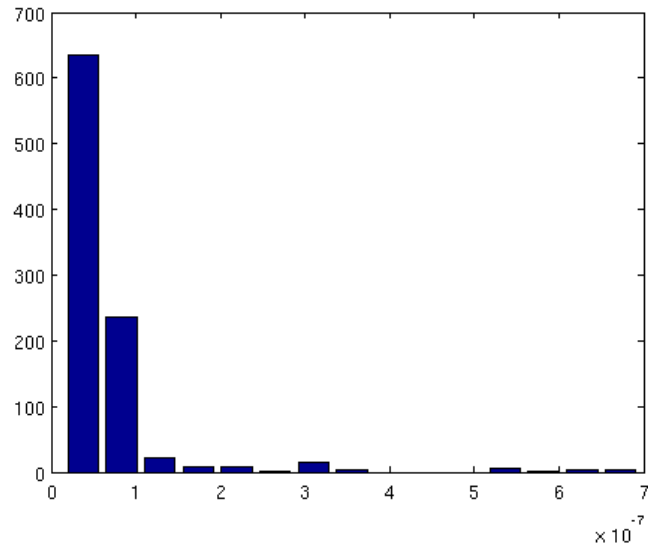


Figure 6.12: Total droplets in L1

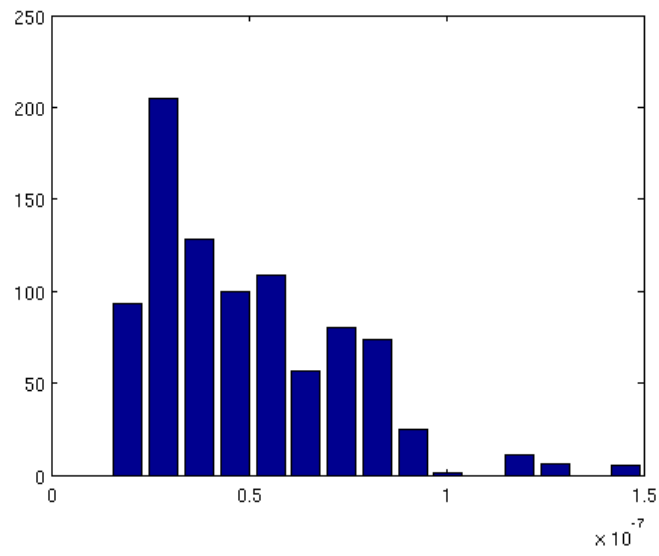


Figure 6.13: Droplets in L1 below $1.5 \cdot 10^{-7} m^3/m$

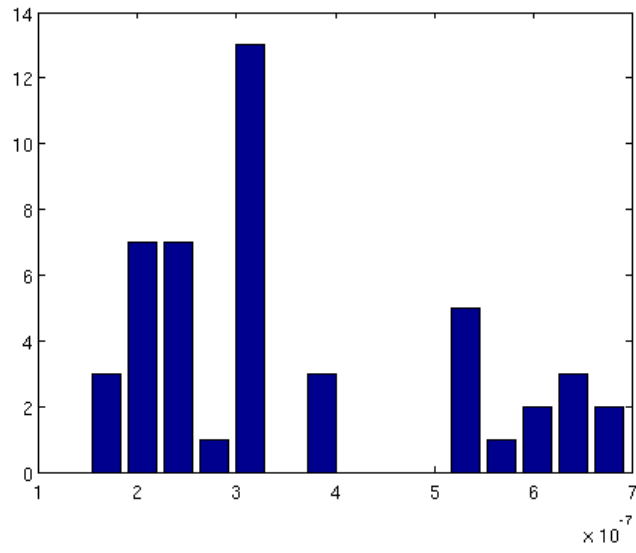


Figure 6.14: Droplets in L1 above $1.5 \cdot 10^{-7} m^3/m$

6.2.2 Simulation L2

Profile	Linear
Average Speed (m/s)	9
Viscosity ($Pa \cdot s$)	$0.65 \cdot 10^{-3}$
Simulation file	L2.gfs
Video file	L2.mpg

Table 6.13: Simulation parameters for L2

Time (s)	Total droplets	Volume detached (m^3/m)	Average droplet size (m^3/m)
0.03	3042	$2.5798e-04$	$5.3486e-08$

Table 6.14: Simulation results of L2

By increasing the speed the entrainment process is intensified, generating 3042 droplets and withdrawing a volume of $5.3486e-08 m^3/m$. This is the reference speed taken in the L4 and L5 cases in which the viscosity changes.

The figure 6.15 illustrates all the droplets formed in the simulation, while the other figures separate the droplets which are bigger and smaller than $1.5e-07 m^3/m$.

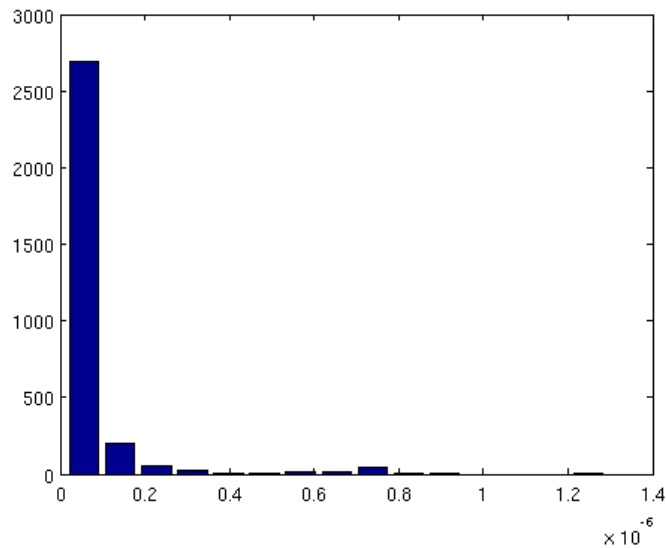


Figure 6.15: Total droplets in L2

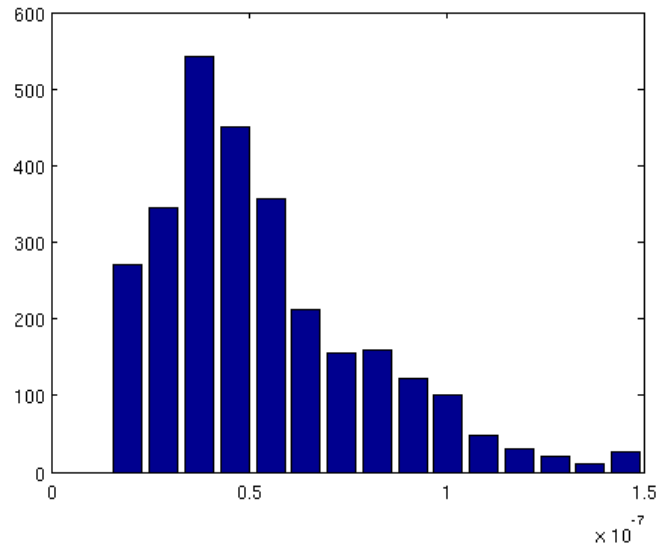


Figure 6.16: Droplets in L2 below $1.5 \cdot 10^{-7} m^3/m$

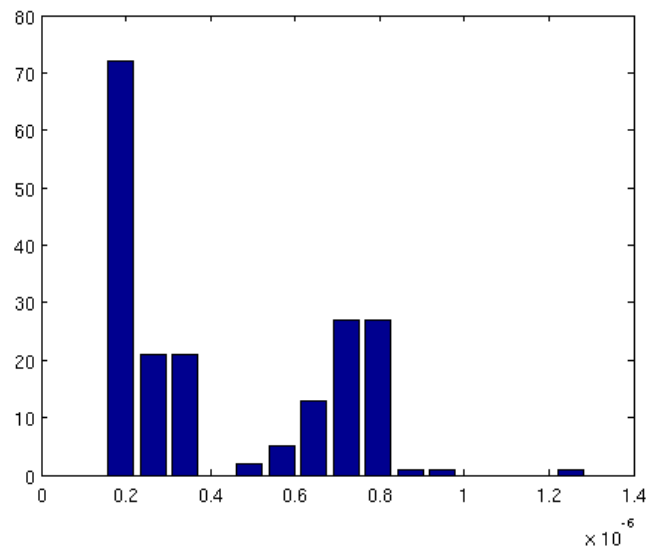


Figure 6.17: Droplets in L2 above $1.5 \cdot 10^{-7} m^3/m$

6.2.3 Simulation L3

Profile	Linear
Average Speed (m/s)	6
Viscosity ($Pa \cdot s$)	$0.65 \cdot 10^{-3}$
Simulation file	L3.gfs
Video file	L3.mpg

Table 6.15: Simulation parameters for L3

Time (s)	Total droplets	Volume detached (m^3/m)	Average droplet size (m^3/m)
0.03	350	$1.3719e-05$	$3.5211e-08$

Table 6.16: Simulation results of L3

Just for checking again that the quantity of droplets is greater as quicker is the flow, a test with an average speed of 6 m/s has been carried out. As expected the entrainment phenomenon is even slighter than in L1 forming just 350 drops and withdrawing a volume of $3.5211e-08 m^3/m$.

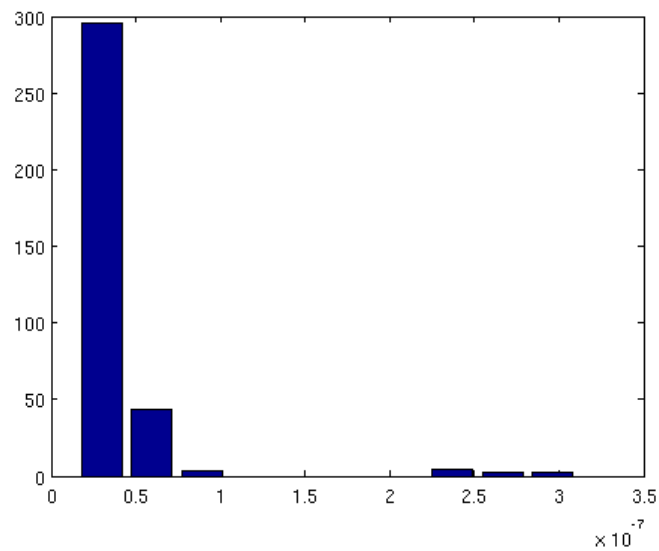


Figure 6.18: Total droplets in L3

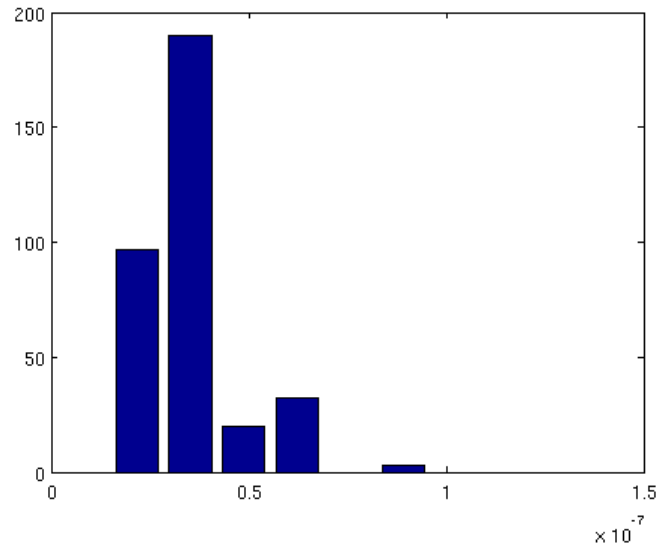


Figure 6.19: Droplets in L3 below $1.5 \cdot 10^{-7} m^3/m$

6.2.4 Simulation L4

Profile	Linear
Average Speed (m/s)	9
Viscosity ($Pa \cdot s$)	0.0034
Simulation file	L4.gfs
Video file	L4.mpg

Table 6.17: Simulation parameters for L4

Time (s)	Total droplets	Volume detached (m^3/m)	Average droplet size (m^3/m)
0.03	4	5.3725e-07	1.3431e-07

Table 6.18: Simulation results of L4

If L2 is taken as reference simulation, conserving the same velocity profile (with $9 m/s$ as average speed) and increasing the dynamic viscosity from 0.00065 to $0.0034 Pa \cdot s$ only four droplets are formed from the paraffin reservoir and no figure is shown then.

6.2.5 Simulation L5

Profile	Linear
Average Speed (m/s)	9
Viscosity ($Pa \cdot s$)	0.000239
Simulation file	L5.gfs
Video file	L5.mpg

Table 6.19: Simulation parameters for L5

Time (s)	Total droplets	Volume detached (m^3/m)	Average droplet size (m^3/m)
0.03	3899	8.1028e-04	5.2050e-08

Table 6.20: Simulation results of L5

If instead of increasing the viscosity it is decreased, the entrainment phenomenon is highly favoured, passing from the 3042 droplets L5 to 3899. Comparing the figures 6.17 and 6.17, it can be concluded that in L5 with lower viscosity the droplets are smaller.

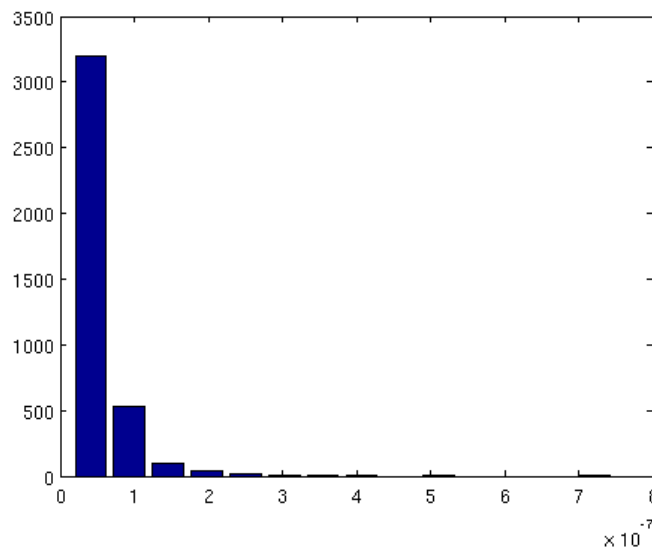


Figure 6.20: Total droplets in L5

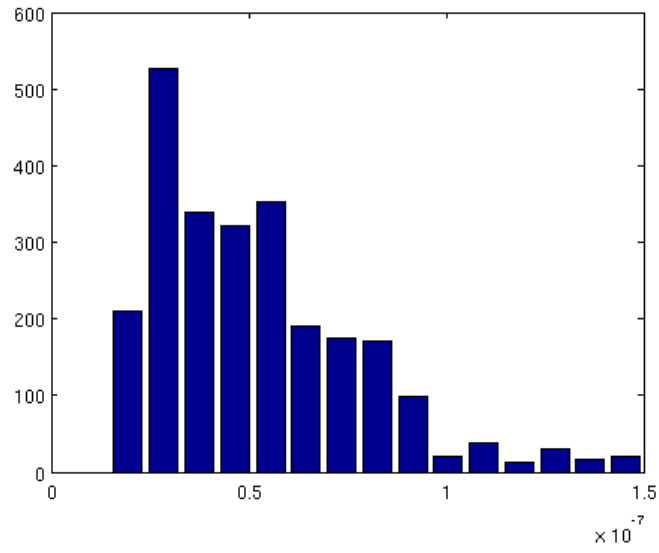


Figure 6.21: Droplets in L5 below $1.5 \cdot 10^{-7} m^3/m$

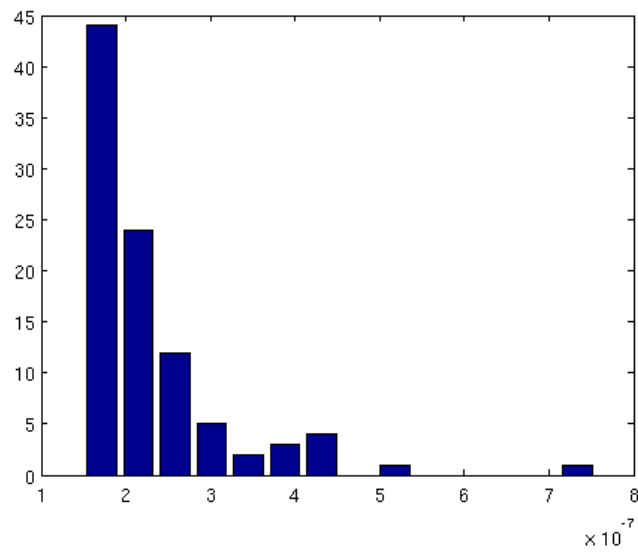


Figure 6.22: Droplets in L5 above $1.5 \cdot 10^{-7} m^3/m$

6.3 Parabolic profile

Finally a parabolic velocity profile for the air has been studied. Firstly, a parabolic profile which velocity was zero in correspondence with the interface was tested, without any results concerning the entrainment phenomenon. Then, in order to develop the entrainment, it has been used a parabolic profile slightly displaced in the Y axis negative direction, so that in correspondance with the interface there is a nonzero speed. Figure 6.23 illustrates this concept.

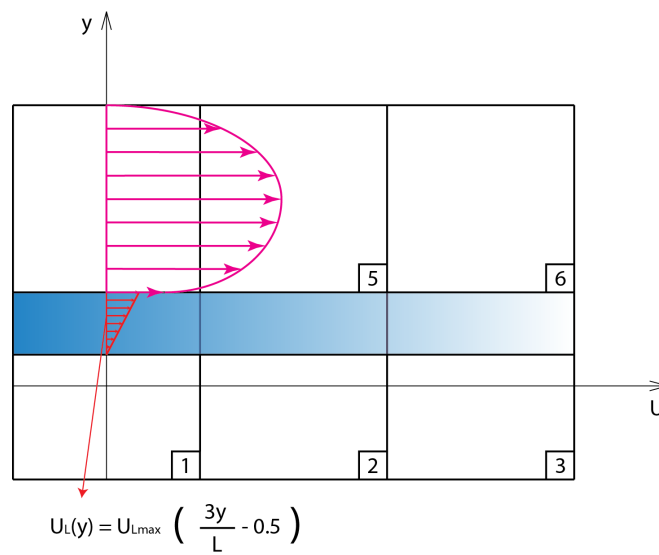


Figure 6.23: Parabolic profile

The equation for the velocity profile is chosen as:

$$U(y) = \left(-4 \frac{U_{input}}{L^2} (y + 0.1L)(y + 0.1L) + 8 \frac{U_{input}}{L} (y + 0.1L) - 3U_{input} \right)$$

In the three first simulations, P1, P2 and P3, different speeds were tested. In the simulations P4 and P5, it has been used the same speed as in case P2, but the viscosity has been increased in P4 and decreased in P5.

6.3.1 Simulation P1

Profile	Parabolic
Average Speed (m/s)	4
Viscosity ($Pa \cdot s$)	$0.65 \cdot 10^{-3}$
Simulation file	P1.gfs
Video file	P1.mpg

Table 6.21: Simulation parameters for P1

Time (s)	Total droplets	Volume detached (m^3/m)
0.05	0	0

Table 6.22: Simulation results of P1

In this first case, with the lowest speed, there is no entrainment at all, as it can be watched in the video file P1.mpg

6.3.2 Simulation P2

Profile	Parabolic
Average Speed (m/s)	7
Viscosity ($Pa \cdot s$)	$0.65 \cdot 10^{-3}$
Simulation file	P2.gfs
Video file	P2.mpg

Table 6.23: Simulation parameters for

Time (s)	Total droplets	Volume detached (m^3/m)	Average droplet size (m^3/m)
0.05	2224	1.5608e-04	5.3568e-08

Table 6.24: Simulation results of P2

Increasing the speed, the entrainment phenomenon is reached. The figure 6.24 illustrates the whole distribution of volumes in the whole simulation. As done before a huge step is present in correspondence with $1.5 \cdot 10^{(-7)}$. So that, in order to highlight the normal distribution in low volumes droplets it has been divided in the droplets which volume is below $1.5 \cdot 10^{(-7)}$ (in figure 6.25) and above that value (figure 6.26).

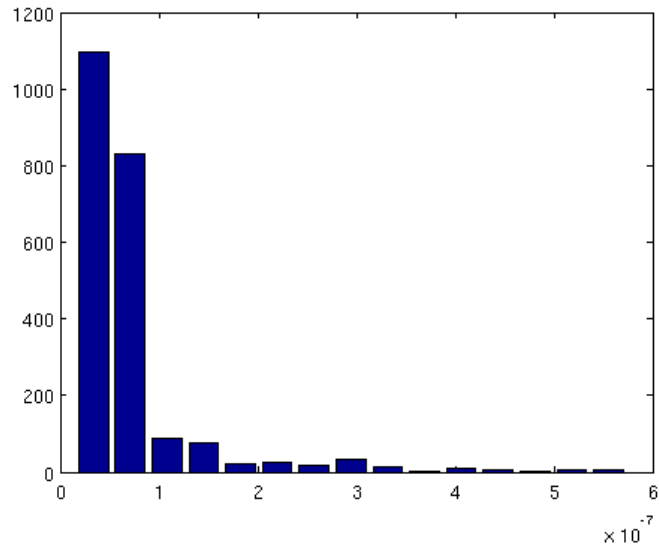


Figure 6.24: Total droplets in P2

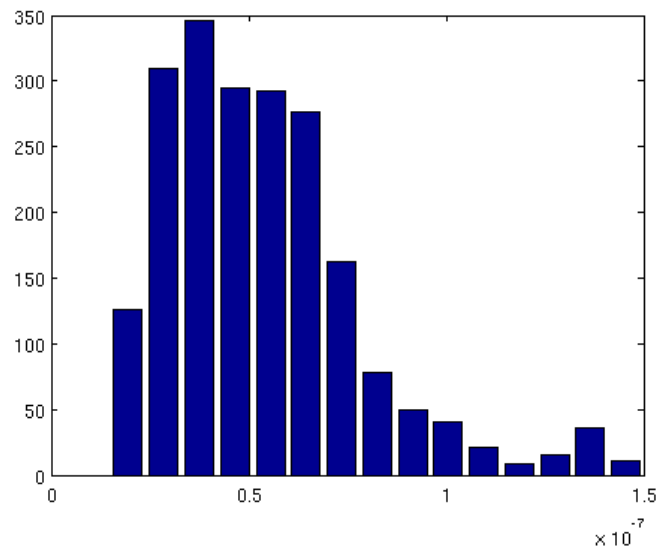


Figure 6.25: Droplets below $1.5e-7 m^2$ in P2

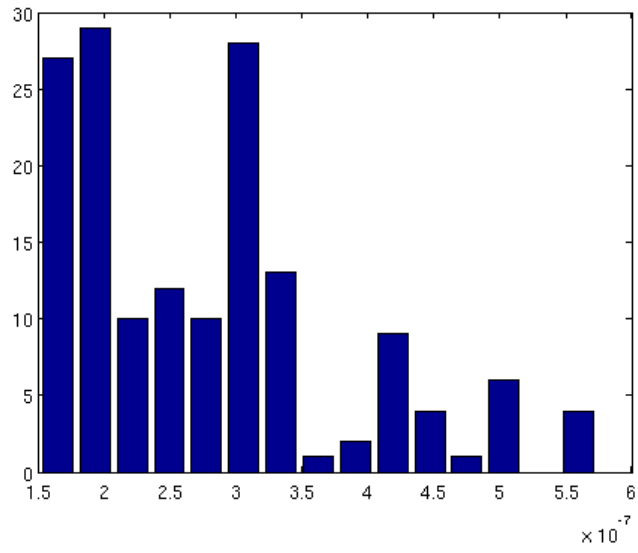


Figure 6.26: Droplets above $1.5 \times 10^{-7} m^2$ in P2

6.3.3 Simulation P3

Profile	Parabolic
Average Speed (m/s)	9
Viscosity ($Pa \cdot s$)	$0.65 \cdot 10^{-3}$
Simulation file	P3.gfs
Video file	P3.mpg

Table 6.25: Simulation parameters for P3

Time (s)	Total droplets	Volume detached (m^3/m)	Average droplet size (m^3/m)
0.05	5468	4.0851e-04	5.6217e-08

Table 6.26: Simulation results of P3

In P3, speed has been increased again. As expectable, the quantity of droplets and the volume detached has increased. It could be said that the parabolic profile is very sensitive to the variation of the speeds, since in this case the droplets formed increased its number in more than 100%. One more time, the simulation is illustrated in three different figures: first one, figure 6.27 all the droplets together and in the figures 6.28 and 6.29 droplets below and above $1.5e-7$ respectively.

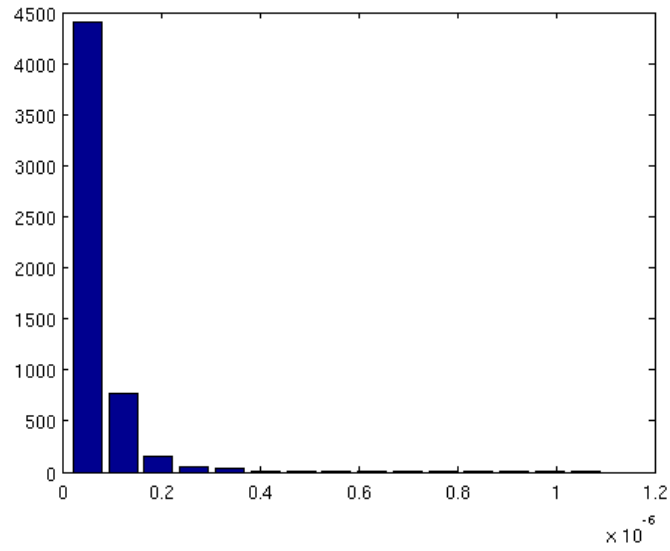


Figure 6.27: Total droplets in P3

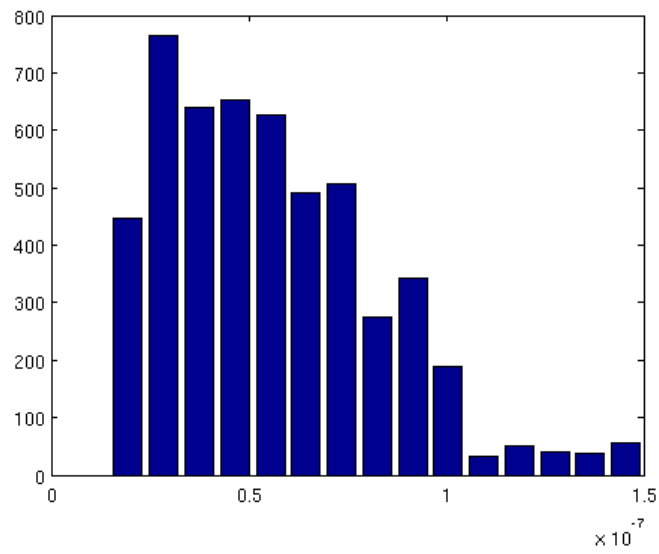


Figure 6.28: Droplets below $1.5e-7 m^2$ in P3

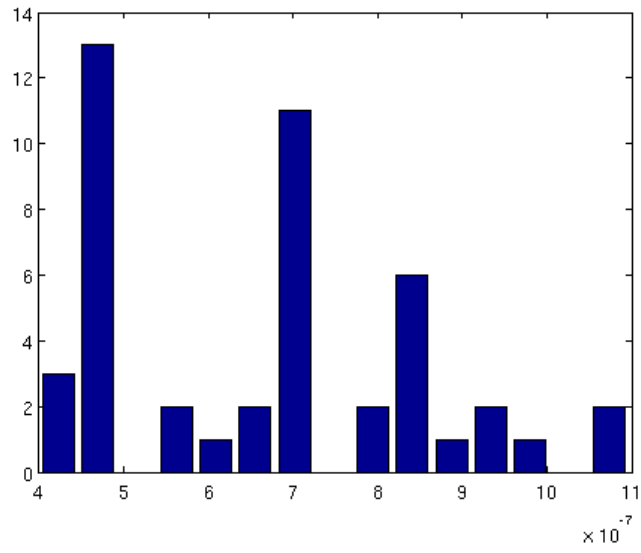


Figure 6.29: Droplets above $1.5 \times 10^{-7} \text{ m}^2$ in P3

6.3.4 Simulation P4

Profile	Parabolic
Average Speed (m/s)	9
Viscosity ($Pa \cdot s$)	0.0034
Simulation file	P4.gfs
Video file	P4.mpg

Table 6.27: Simulation parameters for P4

Time (s)	Total droplets	Volume detached (m^3/m)	Average droplet size (m^3/m)
0.05	281	1.1887e-05	4.230e-8

Table 6.28: Simulation results of P4

At this point, the viscosity has been increased simulating a decrease of the temperature. As expect, once more when the dynamic viscosity takes higher values, less droplets are formed and therefore, less volume detached. This case can be represented well enough in one figure, illustrated below. The samples are very few to fit a normal distribution, but it can be perceived a tendency to it.

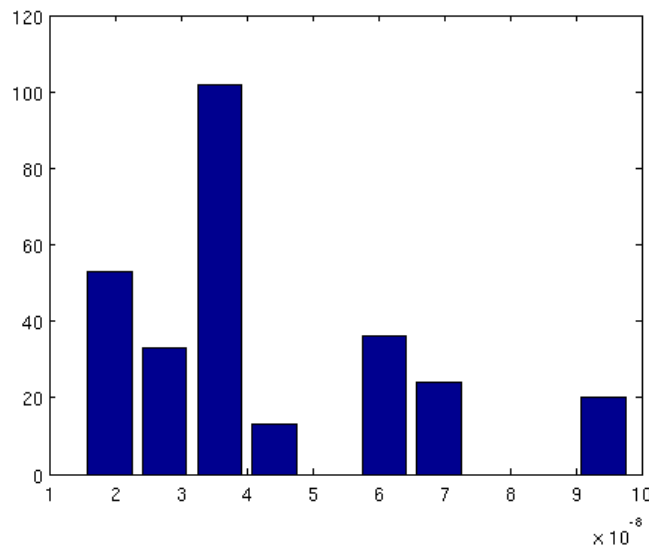


Figure 6.30: Total droplets in P4

6.3.5 Simulation P5

Profile	Parabolic
Average Speed (m/s)	9
Viscosity ($Pa \cdot s$)	0.000239
Simulation file	P5.gfs
Video file	P5.mpg

Table 6.29: Simulation parameters for P5

Time (s)	Total droplets	Volume detached (m^3/m)	Average droplet size (m^3/m)
0.05	971	2.4721e-05	5.3283e-08

Table 6.30: Simulation results of P5

This could be considered exception that proves the rule. While normally when the viscosity is decreased the entrainment phenomenon strengthens itself, this case is the opposite. With this fact it could be concluded that there is an optimal temperature for this kind of profile that maximizes the formation of droplets, and the corresponding viscosity is within the interval $[0.000239, 0.0034] Pa \cdot s$.

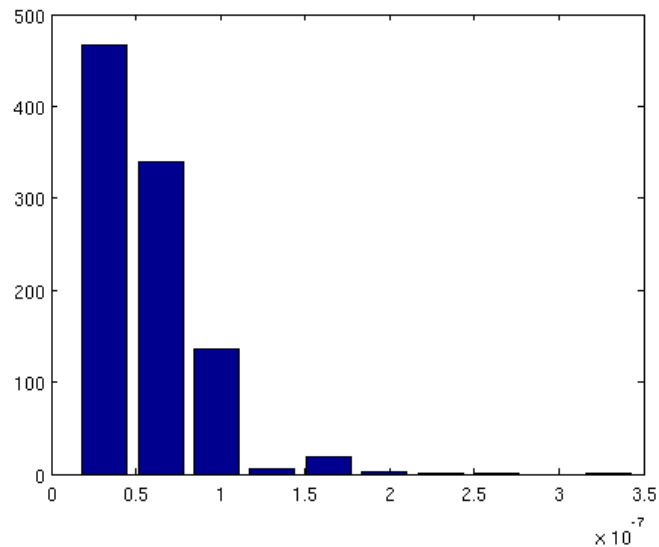


Figure 6.31: Total droplets in P5

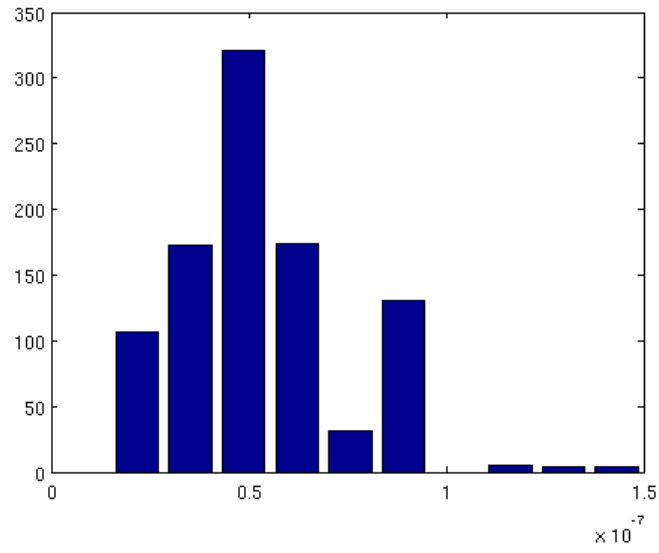


Figure 6.32: Droplets below $1.5 \times 10^{-7} m^2$ in P5

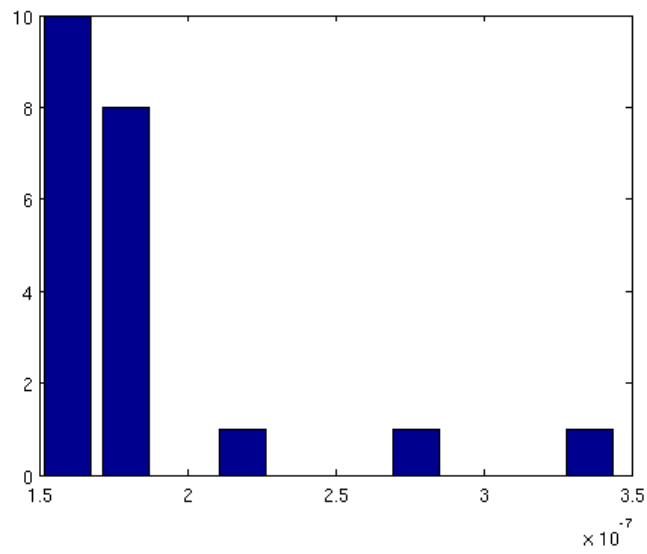


Figure 6.33: Droplets above $1.5 \times 10^{-7} m^2$ in P5

Chapter 7

Conclusions and future work

7.1 Conclusions

7.1.1 Normal distribution on small droplets

In the simulation in which it has proceeded, a division between large and small droplets has been carried out. Comparing all the small droplets distribution in matters of Number of droplets vs Size, the first thing that hits is the shape of the bar graphic which would fit really well to Gaussian distribution.

It is necessary to remove the big droplets in order to observe the similarity with the curve. This fact leads to the thought of two different distributions. The group of droplets whose volume is less than $1.5 \cdot 10^{-7} m^3/m$ tend to a Normal distribution.

It cannot be said the same for the droplets greater than $1.5 \cdot 10^{-7} m^3/m$, whose contribution cannot be neglected because of their size, but they don't form a clear normal distribution even if some of them (for example P2 in figure 6.26) shows a slight tendency to it. There are two explanation to this fact. Firstly the number of samples is very small, few hundreds at most. Then, the nature of this kind of droplets is more like a singular event when a "huge" mass of paraffin is withdrawn from the reservoir.

7.1.2 Number of droplets vs speed

It is very obvious, and it happens in every case that the higher the speed the more intense the entrainment.

For instance in the case of Linear:

Case	Average speed (m/s)	Number of droplets
L1	7	941
L2	9	3042
L3	6	350

Table 7.1: Linear profile comparison

7.1.3 Number of droplets vs dynamic viscosity

For a given speed different values of the viscosity there have been tested for each kind of profile.

When the viscosity has been increased, in every single case, the entrainment phenomenon has high decreased. The explanation is that when the viscosity is higher the temperature is lower, and the paraffin is nearer to the solid state and then it is more reticent to flow. Also, if viscosity is intended as the measure of the resistance of a fluid which is being deformed by shear stress, it could be say that the resistance in this case is very high.

In the cases where the viscosity decreased, it gets more dependent of the profile. In the constant and in the parabolic profile, the number of droplets formed is less that in the original value of the viscosity. In contrast with these cases, in the linear profile, the effect of the increase of the viscosity is different, a higher viscosity makes the entrainment phenomenon more intense generating more droplets.

These two contrasting cases can be explained, in the first instance, when the effect of decreasing the viscosity favours the entrainment, as the weakening of the resistance to be deformed, enough to let the gas withdraw the droplets, and then in the second instance, when the effect of decreasing the viscosity opposes the entrainment, the viscosity is too low that the paraffin better flows rather than be

withdrawn.

To summarize it could be concluded that there is an optimal value of the dynamic viscosity for each different profile that favours the formation of droplets.

7.2 Future work

7.2.1 Computer's performance

One of the main problem of the Volume of Fluid method is the high computational cost when the droplets are formed. A regular simulation of the studied system takes, on average, 7 hours in the computer where it was carried out. The more droplets are formed more difficult is to handle each computational step. When the system is near 200 droplets each computational step takes more than 5 minutes, and each computational step is on the order of microseconds in the actual time step.

Within the documentation of Gerris, it has been found a section that describe the process to run the software in four parallel processors. With this feature, the computational time could be highly decreased letting Gerris to perform a longer simulation.

7.2.2 More velocity profiles

In order to bring up more information, more velocities profiles combined with different values of the viscosity could be used. For example, it could be interesting research about the optimal value of the dynamic viscosity in order to enhance the entrainment phenomenon for each different velocity profile.

Appendix A

Script for filtering first droplet of Gerris output file

```
1 clear all; close all;clc;
2 load vol.dat
3 format shortg;
4 t=vol(:,1);
5 num=vol(:,2);
6 volume=vol(:,3);
7 A=[t num volume];
8
9 %Filters A matrix
10 j=1;
11 i=1;
12 while i<=length(A(:,3))
13     while A(i,2)<1.5
14         i=i+1;
15     end
16     B(j,1)=A(i,1);
17     B(j,2)=A(i,2)-1;
18     B(j,3)=A(i,3);
19     j=j+1;
20     i=i+1
21 end
```

Appendix B

Script for droplets characterization

```
1 clc;clearvars -except B;
2 if exist('B','var')<1
3     drop_filter
4 end
5 time=cputime;
6 N = 15;
7 method = 3 ;
8 if method == 1
9     vol_min = 0 ;
10    vol_max = s ;
11 elseif method == 2
12    vol_min = min( B(:,3) );
13    vol_max = max( B(:,3) );
14 elseif method == 3
15    vol_min = 1e-8;
16    vol_max = max(B(:,3));
17 end
18 p = (vol_max-vol_min)/N;
19 interv = vol_min:p:vol_max;
20 c = zeros(1,length(interv)-1);
21 A=B;
22 i=1;
23 while i<length(A(:,3))
24     u=[];
```


APPENDIX B. SCRIPT FOR DROPLETS CHARACTERIZATION

```
25     v=[];
26     j=1;
27     while i<length(A(:,3))&&A(i,1)==A(i+1,1)
28         u(j)=A(i,3);
29         i=i+1;
30         j=j+1;
31     end
32
33     u(j)=A(i,3);
34
35     i=i+1;
36     trans=i;
37     k=1;
38     while i<length(A(:,3)) && A(i,1)==A(i+1,1)
39         v(k)=A(i,3);
40         i=i+1;
41         k=k+1;
42     end
43     if i<length(A(:,3))
44         v(k)=A(i,3);
45         %v(k+1)=A(i+1,3);
46     end
47     newdroplet=setdiff(roundsd(v,3),roundsd(u,3));
48     for q=1:length(newdroplet)
49         for r=1:length(c)
50             if newdroplet(q) > (vol_min + (r-1)*p) && newdroplet(q)
51                 <= (vol_min + r*p)
52                 c(r)=c(r)+1;
53             end
54         end
55     end
56     i=trans
57 end
```

Appendix C

Function for comparing vectors

```
1
2 function y=roundsd(x,n,method)
3
4 error(nargchk(2,3,nargin))
5
6 if ~isnumeric(x)
7     error('X argument must be numeric.')
8 end
9
10 if ~isnumeric(n) | numel(n) ~= 1 | n < 0 | mod(n,1) ~= 0
11     error('N argument must be a scalar positive integer.')
12 end
13
14 opt = {'round','floor','ceil','fix'};
15 if nargin < 3
16     method = opt{1};
17 else
18     if ~ischar(method) | ~ismember(opt,method)
19         error('METHOD argument is invalid.')
20     end
21 end
22 og = 10.^(floor(log10(abs(x)) - n + 1));
23 y = feval(method,x./og).*og;
24 y(find(x==0)) = 0;
```

Bibliography

- [1] Altman D., Hybrid Rocket Development History, 27th AIAA/ASME/SAE/ASEE Joint Propulsion Conference, 991. AIAA 91-2515.
- [2] Oiknine C., New Perspectives for Hybrid Propulsion, 42nd AIAA/ASME/SAE/ASEE Joint Propulsion Conference & Exhibit, 2006. AIAA 2006-4674.
- [3] Maisonneuve Y. and Lengell G., Hybrid Propulsion: Past, Present and Future Perspectives, Paper 38-1, 6th International Symposium, Proceedings of Propulsion for Space Transportation of the 21st Century, AAAF, 2002.
- [4] Davydenko N.A., Gollender R.G., Gubertov A.M., Mironov V.V. and Volkov N.N., Hybrid Rocket Engines: The benefits and Prospects, Aerospace Science and Technology, Vol. 11, pp. 55-60, 2007.
- [5] Russo Sorge A., State of the Art of Hybrid Propulsion Research in Italy, The 8th International Workshop on Combustion and Propulsion, Naples, 2002.
- [6] Gany A., Scale Effects in Hybrid Motors under Similarity Conditions, AIAA/SAE/ASME 32nd Joint Propulsion Conference and Exhibit, 1996. AIAA-96-2846.
- [7] Evans B.J., Favorito N.A., Boyer E., Risha G.A., Wehrman R.B., and Kuo K.K., Characterization of Nano-Sized Energetic Particle Enhancement of Solid-Fuel Burning Rates in an X-Ray Transparent Hybrid Rocket Engine, 40th AIAA Joint Propulsion Conference and Exhibit, 2004. AIAA 2004-3821.

- [8] Chiaverini M.J., Serin N., Johnson D.K., Lu Y.C. and Risha G.A., Regression Rate Behavior of Hybrid Rocket Solid Fuels, *Journal of Propulsion and Power*, Vol. 16, No. 1, January-February 2000.
- [9] George P., Krishnan S., Varkey P.M., Ravindran M. and Ramachandran L., Fuel Regression Rate in Hydroxyl-Terminated-Polybutadiene/Gaseous-Oxygen Hybrid Rocket Motors, *Journal of Propulsion and Power*, Vol. 17, No. 1, January-February 2001.
- [10] Caravella J.R., Heister S.D. and Wernimont E.J., Characterization of Fuel Regression in a Radial Flow Hybrid Rocket, *Journal of Propulsion and Power*, Vol. 14, No. 1, January-February 1998.
- [11] Chan M. and Johnson C.E., Evaluation of AlH₃ for propellant application, 8-IWPC, Pozzuoli Italy, June 2002.
- [12] Carmicino C., and Russo Sorge A., Role of Injection in Hybrid Rockets Regression rate Behavior, *Journal of Propulsion and Power*, Vol. 21, No. 4, July-August 2005.
- [13] Carmicino C., and Russo Sorge A., Influence of a Conical Axial Injector on Hybrid Rocket Performance, *Journal of Propulsion and Power*, Vol. 22, No. 5, September-October 2006.
- [14] Potapkin A.V. and Lee T.S., Experimental Study of Thrust Performance of a Hybrid Rocket Motor with Various Methods of Oxidizer Injection, Combustion, Explosion, and Shock Waves, Vol. 40, No. 4, pp. 386-392, 2004.
- [15] Risha G.A., Boyer E., Wehrman R.B. and Kuo K.K., Performance Comparison of HTPB-based Solid Fuels Containing Nano-sized Energetic Powder in a Cylindrical Hybrid Rocket Motor, 38 th AIAA Joint Propulsion Conference and Exhibit, 2002. AIAA 2002-3576.
- [16] Risha G.A., Evans B.J., Boyer E., Wehrman R.B., and Kuo K.K., Nano-sized Aluminum- and Boron-based Solid Fuel Characterization in a Hybrid Rocket Engine, 39th AIAA Joint Propulsion Conference and Exhibit, 2003. AIAA 2003-4593.

- [17] Karabeyoglu M.A., Cantwell B.J. and Altman D., Development and Testing of Paraffin-based Hybrid Rocket Fuels, 37th AIAA Joint Propulsion Conference and Exhibit, 2001. AIAA 2001-4503.
- [18] Karabeyoglu M.A., Altman D. and Cantwell B.J., Combustion of Liquefying Hybrid Propellants: part 1, General Theory, Journal of Propulsion and Power, Vol. 18, No. 3, May-June 2002.
- [19] Karabeyoglu M.A., Zilliac G., Cantwell B.J., De Zilwa S. and Castelluci P., Scale-up Tests of High Regression Rate Liquefying Hybrid Rocket Fuels, 41st AIAA Aerospace Sciences Meeting and Exhibit, 2003. AIAA 2003-1162.
- [20] Boffa N.D., Carmicino C., Piloni G., Russo A., Design and Preliminary tests of a HTP/HDPE hybrid rocket for de-orbit manoeuvring, 54th International Astronautical Congress, 2003.
- [21] Carmicino C., Russo A., Combustion gases experimental tests and numerical analysis on a linear plug nozzle, 7th T. I.S. on Fluid Control, Measurement and Visualization, 2003.
- [22] Carmicino C., Russo A., Experimental analysis of the fuel regression rate dependence on pressure in a hybrid rocket, XVII Congresso Nazionale AIDAA, 2003.
- [23] Carmicino C., Russo A., Investigation on the Fuel Regression Rate Dependence on oxidizer Injection and Chamber Pressure in a Hybrid Rocket, AIAA 2003-4591, 2003.
- [24] Milos F.S., and Rasky D.J., Review of Numerical Procedures for Computational Surface Thermochemistry, Journal of Thermophysics and Heat Transfer, Vol. 8, No. 1, 1994.
- [25] Kuntz D.W., et al., Predictions of Ablating Hypersonic Vehicles Using an Iterative Coupled Fluid Thermal Approach, Journal of Thermophysics and Heat Transfer, Vol. 15, No. 2, 2001.

- [26] Sankaran V., Computational fluid dynamics modeling of hybrid rockets flow-fields combustion, *Fundamentals of hybrid rocket combustion and propulsion*, edited by M. Chiaverini and K. K. Kuo, *Progress in Aeronautics and Astronautics*, Vol. 218, 2007.
- [27] Westbrook C.K., and Dryer F.L., Simplified reaction mechanism for the oxidation of hydrocarbon fuels in flames, *Combustion Science and Technology*, Vol. 27, 1981, pp. 31-43.
- [28] Casalino L., and Pastrone D., Optimal Design of Hybrid Rocket Motors for Launchers Upper Stages, *Journal of Propulsion and Power*, Vol. 26, pp. 421-427, ISSN: 0748-4658, doi: 10.2514/1.41856, 2010.
- [29] Pastrone D., Casalino L., Rosa Sentinella M., and Carmicino C., Acoustic Analysis of Hybrid Rocket Combustion Chambers, *Journal of Propulsion and Power*, Vol. 26, pp. 415-420, ISSN: 0748-4658, doi: 10.2514/1.39578, 2010.
- [30] Casalino L., Colasurdo G., and Pastrone D., Integrated Design of Hybrid Rocket Upper Stage and Launcher Trajectory, 45th AIAA/ASME/SAE/ASEE Joint Propulsion Conference and Exhibit, 2009.
- [31] Arif Karabeyoglu. (May 09, 2008). Hybrid Rocket Propulsion for Future Space Launch. In *University of Stanford*. Retrieved Feb 27, 2012, from <http://aa.stanford.edu/events/50thAnniversary/media/Karabeyoglu.pdf>